International Journal of Mechanical Sciences 223 (2022) 107236

Contents lists available at ScienceDirect

International Journal of Mechanical Sciences

journal homepage: www.elsevier.com/locate/ijmecsci

A physics-informed multi-agents model to predict thermo-oxidative/hydrolytic aging of elastomers

Aref Ghaderi [a], Vahid Morovati [b], Yang Chen [a], Roozbeh Dargazany [a,*]

[a] Department of Civil and Environmental Engineering, Michigan State University, United States of America
[b] Department of Aerospace Engineering and Engineering Mechanics, University of Texas at Austin, United States of America

ARTICLE INFO

Keywords:
Data-driven constitutive modeling
Neural networks
Thermo-oxidative aging
Hydrolytic aging
Multi-agent system

ABSTRACT

This paper introduces a novel physics-informed multi-agents constitutive model to propose prediction in quasi-static constitutive behavior of cross-linked elastomer and the loss of mechanical performance during environmental aging. The presented model is used to simulate the effect of single-mechanism chemical aging (i.e. thermal-inducedor hydrolytic aging) on the behavior of the material in this hybrid framework. Those environmental single-mechanism damages change the polymer matrix over time due to massive chain scission, chain formations, and changing the arrangement of molecules in the polymer matrix. We propose a data-driven super-constrained machine-learned engine to represent damage in the polymer matrix and capture the changes in material behavior, including its inelastic features such as Mullins effect and permanent set in the course of aging. We have simplified the 3D stress–strain tensor mapping problem into a small number of super-constrained 1D mapping problems by means of a sequential order reduction. An assembly of multiple replicated conditional neural-network learning-agents (L-agents) is trained to systematically simplify the high-dimensional mapping problem into multiple 1D problems, each represented by a different type of agent. Our hybrid framework is designed to capture the effect of deformation history, aging time, and aging temperature. The model is validated with respect to a comprehensive set of experiments specifically designed to benchmark model capabilities and also against available data in the literature. Thermodynamic consistency and frame independency have been verified. Besides acceptable predictive abilities, a significant reduction of computational cost to predict behavior at multiple states of deformation is the most significant feature of this model.

1. Introduction

Nowadays, cross-linked elastomers play a significant role in several industries such as aerospace, structure, transportation, shipbuilding, and automotive due to excellent flexibility, toughness, form-ability, and versatility, [1,2]. These materials encounter aggressive environmental conditions such as water, temperature, and solar ultraviolet radiation (UV) during their operation, which affects their durability and properties. Fig. 1 shows common forms of aging.

Over the last four decades, many degradation studies have dealt with the complexity of polymer lifetime prediction and extrapolations, either by measuring mechanical or similar degradation indicators over a large temperature range, thereby establishing the basis for predictions, or by focusing on limitations in straight line Arrhenius extrapolations. It is interesting to note how trends in these studies over the years reflect on the evolution of more sensitive analytical techniques, better stabilization of materials, and an overall improved understanding of polymer aging phenomena [3–6].

The reliable design of rubbery structures, which prevents failure due to environmental degradation, requires the development of constitutive models considering the high stretching capacity in different states of deformation. This can be achieved through continuum-based models integrating the relationship between the large-strain macro-response and the degradation processes, all of which are of crucial importance. In this regard, it is the main goal of this study to propose a practical and simple description of the environmental aging of rubbery media through a novel constitutive model using physically realistic approaches. In this study, we try to use machine learning algorithms that need the minimum possible dataset for training. It is axiomatic that the predictability of the model is related to the dataset size that we are using for training.

* Corresponding author.
E-mail addresses: ghaderi1@msu.edu (A. Ghaderi), morovati@austin.utexas.edu (V. Morovati), chenya36@msu.edu (Y. Chen), roozbeh@msu.edu (R. Dargazany).

https://doi.org/10.1016/j.ijmecsci.2022.107236
Received 30 August 2021; Received in revised form 22 February 2022; Accepted 23 March 2022
Available online 9 April 2022

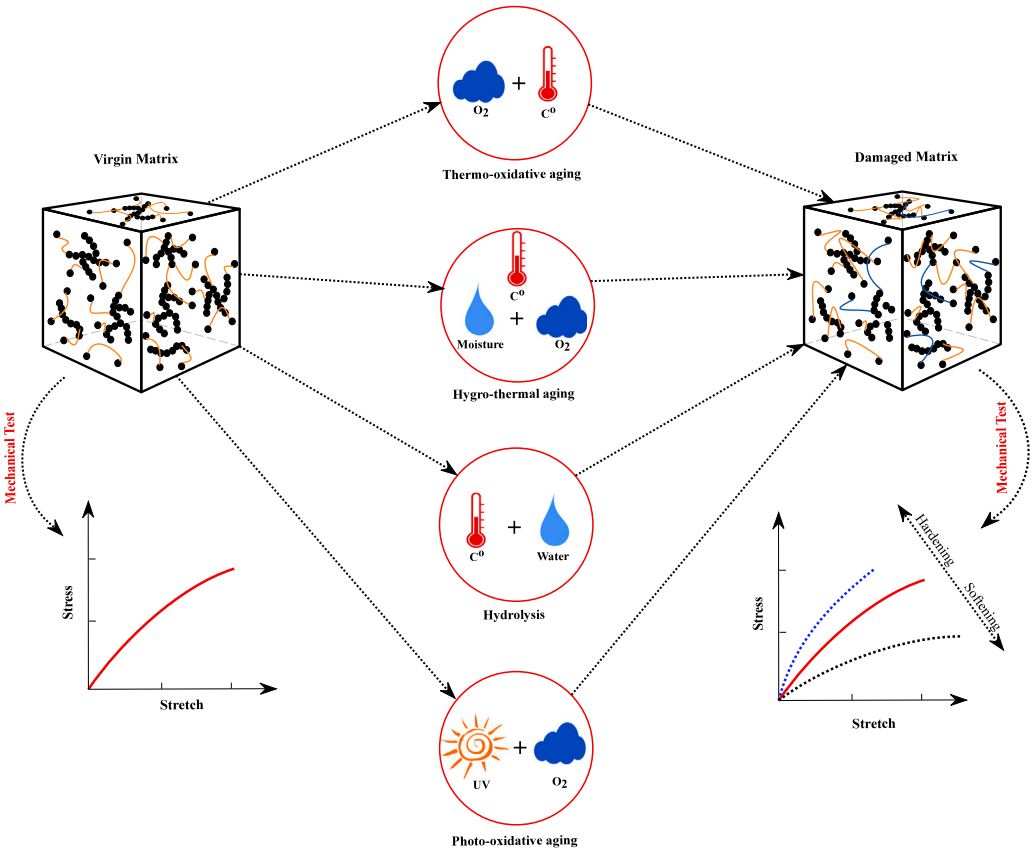

Fig. 1. Schematic of common types of aging including thermo-oxidative, hygrothermal, hydrolysis, and photo-oxidative agings.

Polymer aging can take form in either physical or chemical changes or both. Notable examples of chemical changes that occur due to weathering are chain scission during the curing of polymers, thermal conditioning at elevated temperatures, and photo-chemical aging. In polymeric systems, physical aging refers to the structural relaxation of the glassy state toward the meta-stable equilibrium amorphous state and it is accompanied by changes in almost all physical properties. Specifically, physical aging occurs when the material is in a non-equilibrium state, and gradually tends towards an equilibrium due to the macromolecular relaxation; Note that the proposed model in this paper does not consider high-temperature aging and is just valid for a small range around glass transition temperature (T_g). Temperature elevation can often accelerate physical aging and is often used for this purpose since real-time physical aging is super-slow, which makes it often infeasible for most studies.

Higher temperatures can also accelerate chemical reactions of the matrix in the presence of oxidizing agents like oxygen, which causes chemical aging of the system. The collection of the physical and chemical changes induced by time at high temperatures is often known as thermal-induced oxidative aging. The polymer matrix changes during thermal-induced aging as the polymer backbone interacts with oxygen. There are two main consequences of chemical reactions at the macromolecular scale: (i) polymer chain scission and (ii) cross-link formation. The contribution of those two mechanisms to the behavior of the aged material will increase along the aging period; the resulting state of the material can be considered a product of the competition between these reactions. The change can be dominated by either reaction depending on the polymer matrix type, cross-linking agents, and the aging temperature. Generally, the increase of cross-link density significantly increases the matrix stiffness, increases T_g, and reduces its stretchability. Both reactions have a substantial effect on the polymer chain length distribution within the matrix as well. Additionally, aging alters the arrangement of molecules in the polymer matrix. [7,8].

In the presence of water, such as in the case of submerging polymer samples in water, hydrolytic aging can take place. The interaction of the elastomer matrix with the hydroxyl or hydrogen ions in water causes hydrolytic aging. Chain scission and chain detachment may occur as a result of water molecules attacking the polymer matrix hydrolytically. Hydrolytic attacks, on the other hand, reduce the molecular weight of the matrix, which also affects the mechanical behavior [9]. Generally, short-term aging is attributed to the materials that need curing, such as adhesives. This phenomenon is also referred to over curing as well [10]. In this respect, here we used cured specimens to avoid over-curing in our aging setup. During thermo-oxidative aging, two simultaneous phenomena will occur, which are namely chain scission and cross-link formation. In most of the cross-linked polymers such as SBR, crosslink formation is dominant, which made the material tougher. On the other hand, during hydrolytic aging, chain scission is dominant, and as a result, water acts as a plasticizer, and as a result, makes the material softer. From the constitutive modeling point of view, constitutive behavior is mainly getting harder by thermo-oxidative aging while hydrolytic aging makes it softer [11].

There are other types of aging, such as (i) hygrothermal aging, which is a coupled concurrent effect of thermal-induced and hydrolysis aging, and (ii) photo-oxidative aging, which is accelerated thermal-induced aging with UV (see Fig. 1). Many experimental and theoretical models have been proposed in order to show the effect of thermal-induced and hydrothermal aging on the mechanical behavior of cross-linked elastomers.

In experimental approaches, three types of tests are used to characterize the mechanical behavior of elastomers during "single-mechanism chemical" aging;

(i) **Relaxation test**, where the temperature and strain of samples are held constant during the aging, and the stress drop is studied over time (Fig. 2.a).

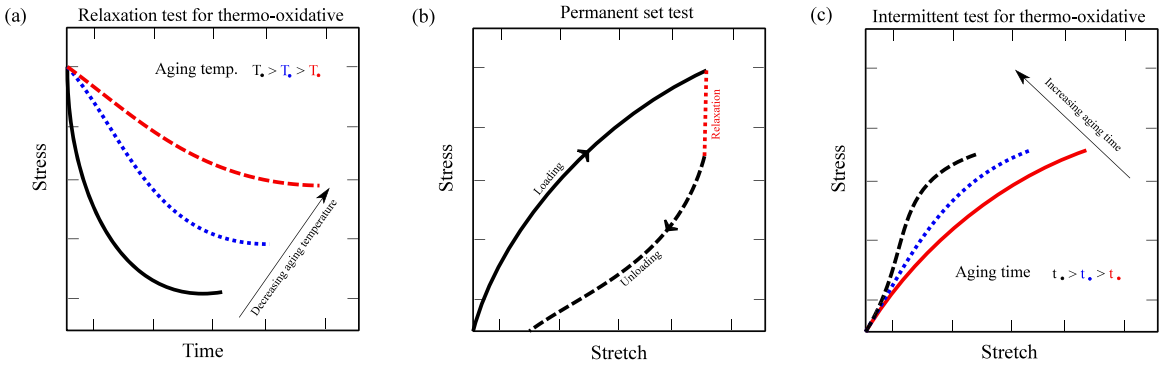

Fig. 2. Schematic illustration of (a) intermittent test (b) relaxation test (c) permanent set test for thermo-oxidative aging [29].

(ii) **Permanent set test**, which is similar to the relaxation test, but after relaxation, the specimen is unloaded, and the final length is measured and investigated with initial length (Fig. 2.b).

(iii) **Intermittent test**, where the sample is aged at stress-free state first and then characterized [12] (Fig. 2.c).

Several studies have investigated thermal-induced aging through those tests for different types of materials, such as natural rubber [13–18], and composites [19–21]. Similarly for hydrolysis, those tests were used to characterize aging in rubbers, [22–24], composites [25,26], and biodegradable materials [27,28].

In theoretical approaches, researchers usually combine hyperelastic constitutive models, which describe the hyperelastic behavior of materials irrespective of the effects of aging time and temperature, with degradation models, which demonstrate the decay of materials during aging. Rubber elasticity theory is driven partly based on (i) statistical mechanics at micro-scale (ii) Phenomenological Modeling at Meso-scale for modeling of the network (iii) Continuum Mechanics at Macro-scale to model the material. So, hyperelastic models fall into three main categories: the phenomenological approach, the micro-mechanical approach, and the data-driven approach. In the first one, a mathematical model is considered without any physical interpretation, and model parameters are fitted by experimental data set. Ogden's model [30], the Neo-Hooken [31], Yeoh's [32], Mooney–Rivlin's [33], Gent's [34], Carroll's [35], and Swanson's models [36] are well-known examples in this category. These phenomenological models, with a set of material parameters, do not employ the micro-physics behind materials. The micro-mechanical approach is based on statistical mechanics of polymers structure and employs physical meaning during analysis. Thus, some of them can show inelastic behaviors of cross-linked elastomers, such as the Mullins effect and permanent set. Three-chain model [37], eight-chain [34], full network [38], extended tube [39], non-affine micro-sphere [40], network alteration [41], and network evolution models [1,42] are the most famous models in this category. Micro-mechanical models, with functions and material parameters related to micro-structure, consider micro-structural information [43]. However, given the complexity of these models, their practical application is limited due to their huge computational costs and complex training process. Quite recently, Amores et al. [44–46] proposed a new projection of stretch using the right stretch tensor that significantly improves the behavior of the micro-sphere models. They hypothesized that the equivalent fluctuation-free network could be obtained by this projection or its extension. Their model can be trained with a similar number of experiments as in other structure-based models but have less accuracy and the same computational complexity similar to closed-form or pre-integrated models. For more information, please see [47,48]; Dal et al. evaluated the strength and weaknesses of 44 hyperelastic constitutive models for elastomers under uniaxial, pure shear, and equi-biaxial deformations.

In recent decades, the emergence of machine-learned (ML) models has attracted much attention. The first generation of "black-box" ML models as another type of phenomenological model was proposed to model the mechanical behavior of rubbery media [49,50]. It is worth noting that the high degree of freedom of these approaches makes them obsolete due to the high demand for data for training.

In solid mechanics, stress–strain tensors are only partially observable in lower-dimensions. Thus, obtaining data to feed a black-box ML model is exceptionally challenging. Thus, in the next generation of ML models, physics-informed neural networks (PINN) combine the best of the two mentioned worlds. In other words, PINN as a hybrid framework attempts to address the limitations of both phenomenological and micro-mechanical models by obtaining micro-structural behavior from the macroscopic experimental data set [51,52].

Model-free distance minimization methods have been designed to avoid the need for constitutive models by explicitly identifying stress–strain pairs with the shortest distance to experimental data while still satisfying compatibility and equilibrium constraints [53,54]. Dimension-reduction methods attempt to construct a constitutive manifold from experimental data in order to explain a close approximation of the strain energy in various states of deformation [55,56]. ML models are used as surrogate functions in autonomous approaches to capture the high-dimensional and non-smooth micro-scale action of material constituents, which has been shown to be a promising method in multi-scale analysis [57,58]. Furthermore, using the principle of network decomposition, we recently proposed a neural network method that predicts not only different states of deformation but also the inelastic behavior of cross-linked elastomers [59–61].

In recent decades, the phenomenon of degradation has attracted wide attention; Scholars have proposed different mathematical degradation models based on their applications. The Arrhenius along with the [62] Archard [63] and Paris models, [64] fall in single mechanism degradation, which is continuous and without any fluctuation. Several models have been proposed from a combination of constitutive models and degradation models. Ha-Anh and Vu-Khanh [65] employed an Arrhenius function and combined it with the Mooney–Rivlin model to predict the hyperelastic behavior of aged polychloprene. Lion et al. [12] proposed a phenomenological model by splitting Helmholtz free energy into three parts. In 2013, Johlitz [66] proposed a phenomenological model that considers both mechanical and chemical degradation. Meanwhile, in the micro-mechanics category, Mohammadi et al. [7,67] proposed a model for thermal-induced aging that combined the Author's network evolution model with the Arrhenius function and different decay rates. This study [68] investigated the geometry dependency of aging between substrate and adhesive by employing finite element simulation based on chemo-mechanical modeling. There are a few models that theoretically investigate hydrolysis [69]. Viera et al. [70] proposed a model for hydrolysis using Bergstrom and Boyce's constitutive model by decomposing mechanical behavior into time-dependent and time-independent parts. In another study, the Author investigated the mechanical behavior of biodegradable materials during hydrolysis aging by employing a quasi-linear viscoelastic model [71]. In another

micromechanical study, Bahrololoumi et al. [11] proposed a model for hydrolysis that combined Author's network evolution model and Arrhenius decay function. All the mentioned models have several advantages and disadvantages.

Micromechanical approaches are highly interpretable but complex because they consider the readjustment of kinks, the rearrangement of convolutions, reorientation, and the uncoiling of molecular chains. Phenomenological approaches are empirical, easy, and less interpretable; however, micromechanical approaches are highly interpretable but complex because they consider the readjustment of kinks, the rearrangement of convolutions, reorientation, and uncoiling of molecular chains. Meanwhile, the emergence of machine-learned (ML) models has attracted much attention as a way to address the mentioned challenges of the phenomenological and micromechanical approaches.

The three key novelties of the proposed methodology are:

- Despite wide range of studies on behavior of elastomers behavior during aging and abundance of data, there has been very few physics-informed data-driven models that can successfully reproduce the experimental data other than those used for training.
- So far, data-driven constitutive model for single-mechanism aging are mostly based on black-box approach and there has been no methodology to infuse background knowledge into the modeling to reduce the dependency on data.
- A comprehensive data-driven model for aging problems are strictly limited to few simple studies.

In view of those challenges, we proposed a new approach for reduced order modeling single-mechanism aging in elastomers by infusing Knowledge into a data-driven approach. The following are the major novelties of the proposed method:

(i) Developed a systematic approach to reduce order of the constitutive mapping and address data volume problem for training.

(ii) Validated a novel physics-informed hybrid framework to describe the relationship between elastomeric network mechanics and environmental degradation.

(iii) Predicted various inelastic effects through our model which is also less data-dependent, has higher interpretability, and uses a knowledge confined solution space.

(iv) Incorporating background knowledge from polymer physics, continuum mechanics, and thermodynamics into the neural networks and constraint the solution space.

Therefore, in this contribution, we develop a hybrid physics induced data-driven framework that is constrained and simplified by applying rules and concepts from polymer physics, continuum mechanics, and thermodynamics to predict the effects of a single mechanisms environmental aging such as thermal-induced aging or hydrolysis on constitutive behavior of the material. The proposed model is based on the concept of a cooperative multi-agent system $\mathcal{A}_j^i$, $i \in \{1, n\}$, $j \in \{1, m\}$ to describe different features in the material behavior with $n \times m$ different neural network learning agents (L-agents), which are responsible for learning from experimental data sets. We have simplified the 3D stress–strain tensor mapping problem into a small number of super-constrained 1D mapping problems by means of a sequential order reduction. We assume that during aging, the polymer matrix is changed by degradation, and due to the lack of exact knowledge on behavior and interaction of polymer microstructures, we model it using an L-agent system. The model is validated by our set of experimental data. In addition, relaxation and intermittent experimental data available in the literature are used to show the proposed model's accuracy in different conditions. The hybrid NN model can predict aging behavior between the lowest and highest temperature. Although in NNs, we can control it, so it is only valid in the domain it is trained. The reason is that we have not implemented physical equations in the proposed hybrid model. It is our outlook for future study.

The rest of this manuscript is organized as follows. In Section 2, deformation and aging-induced damage of polymer matrix are explained physically in detail. Next, we demonstrate strain energy function extraction based on a cooperative multi-agent system. We explain the proposed model in detail in Section 3. In Section 4, results of the proposed model are presented to show the goodness and performance of the model. Finally, the conclusion is provided in Section 5.

2. Mechanical and environmental damages in polymers

Cross-linked elastomers are created by mass cross-linkage of polymer macro-molecules to each other within a confined space. Modeling the constitutive behavior and damage mechanisms in cross-linked polymers has been the subject of interest for the past 50 years, and a general description of the micro-processes has been formulated. In general, elastomer degradation is caused by two types of stresses: mechanical, such as deformation, vibration, and relaxation, and environmental, such as thermal aging, hydrolysis, and photo-oxidation.

Deformation-induced damage: One good example of mechanical damages is the Mullins effect, where the matrix softens after the first stretch [72–74]. This phenomenon happens in filled rubber polymers, not all polymers. There are multiple sub-structural changes in the matrix that are formed due to mechanical damages, such as chain breakage in the filler interface, chain disentanglement, molecules slipping, and rupture in the cluster of fillers [75,76], which are summarized in Fig. 3.

Environmental damage occurs mostly due to changes in the chemical micro-structure of the matrix, which occurs due to competition or collaboration of multiple sub-mechanisms. For example, thermal aging is widely considered as the competition between cross-link formation mechanism and chain scission mechanisms, where the former makes the matrix stiffer by inducing new bonds. In contrast, the latter makes it softer by debonding polymer chains from the system (Fig. 3). The rate of polymer chain scission and cross-links formation defines that the material should become brittle or ductile, although in both cases, the matrix experiences damage [77].

Thermo-oxidative kinetics: During thermo-oxidative aging, the rate of chemical oxidation can be characterized as

$$-\frac{d[P]}{dt} = k[P]^q, \tag{1}$$

$[P]$ is the chemical compound concentration of P, k is the reaction rate coefficient, and q is the reaction order. The chemical reaction governing a degradation process is commonly described using first-order kinetic equations ($q = 1$). Furthermore, k is just a function of temperature in the presence of homogeneous conditions, low stretches during aging, and no diffusion-limited oxidation. The major cause of alterations in the polymer matrix is chemical interactions between the polymer backbone and oxygen during thermal-induced aging [78–80].

Hydrolysis kinetics: Hydrolysis is commonly described using first-order kinetics equations, similar to thermal-induced aging, but with respect to the production rate of carboxylic end groups.

$$\frac{d[C]}{dt} = \zeta[C], \tag{2}$$

where $[C]$ is the carboxyl end group content in the polymer matrix. The parameter ζ is the hydrolytic degradation rate, which determines the rate at which the material ages. Mechanical stress, ester group condensation, polymer structure, water diffusion, temperature, and the pH of the degradation environment are all elements that influence the rate of degradation. As a result, applying mechanical stress during hydrolytic degradation might increase the likelihood of chain cleavage and, as a result, the hydrolysis rate constant. Similarly, the pH of the degrading environment can influence the hydrolysis rate constant via catalysis. Due to the absence of mechanical force, constant temperature, and constant pH in the domain, the hydrolysis rate remains constant through the degradation process in this investigation. Furthermore, as compared to hydrolytic aging, the time spent diffusing water into the sample volume is insignificant. In fact, the water was evenly distributed across the sample volume. As a result, during the course of the degradation process, the concentration of water molecules is considered to

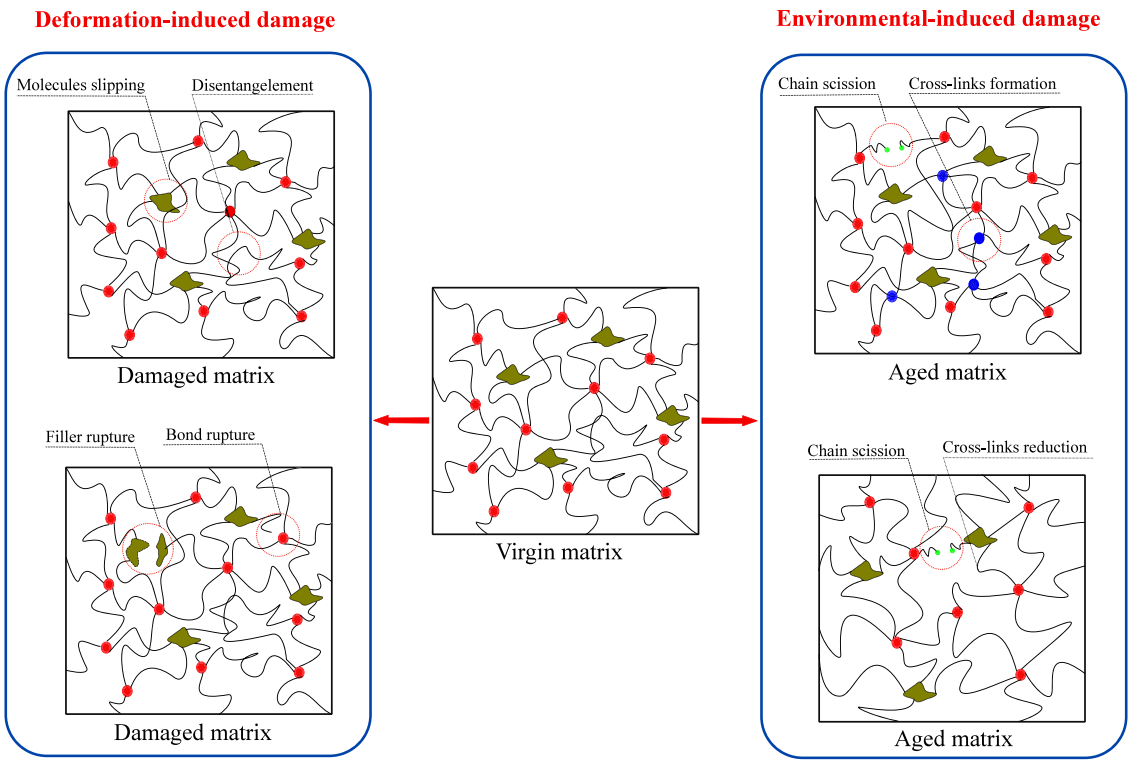

Fig. 3. Schematic of polymer matrix change alongside with deformation-induced and environmental-induced damage. Deformation-induced damages include breakages of chain crosslinks, chain scission, bond rupture, desorption of chains, slippage of chains, absorption of chains, and filler rupture. Environmental-induced damages include chain scission, crosslinks formation and reduction.

remain constant. To make the formulation easier, the deterioration rate is assumed to remain constant throughout the aging process at a given temperature θ [81,82].

3. Physics-constrained data-driven modeling: Multi-agents model

Overview. This work presents a new generation of *super-constrained deep-learned hybrid constitutive models* that can describe the accumulated effects of the mechanical and environmental damage on elastomer Matrix. The model describes the matrix through a cooperative multi-agents framework where each agent has been defined by a simple deep-learned neural network (NN) which is super-constrained by equations derived from physics, thermodynamics, and continuum mechanics. The use of NN agents within the micro-mechanical models, as opposed to traditional physics-driven modeling methods, provides a new generation of hybrid models that use the interpretability/simplicity of micro-mechanical models plus the computational speed and adaptability of machine-learned algorithms. While the accuracy of the predictions of the proposed hybrid model still relies heavily on the quality of the data used for training, the model output is already constrained within the region that satisfies our existing knowledge of the matrix behavior.

The model has been constrained at multiple steps; (1) model defined based on strain energy; (2) hiring micro-sphere for 3D to 1D order reduction; (3) using network decomposition to separate different inelastic effects; (4) defining learning agents to represent each 1D subnetwork. Those steps which are required to build a cooperative multi-agents hybrid model and their formulation are outlined in the following.

3.1. Cooperative multi-agents system

In finite deformation regimes, strain–energy based constitutive functions are extremely advantageous over classical stress–strain equations by satisfying multiple conditions at once, such as normalization, growth conditions, isotropy, objectivity, and poly-convexity to ensure the solution's uniqueness (Appendix). Moreover, strain energy based formulations can be easily verified against the 2nd law of thermodynamics and consequently Clausius–Planck inequality by being formulated with respect to different work conjugate pairs such as

$[(\mathbf{F}: deformationgradient, \mathbf{P}: firstPiola--Kirchhoffstress),$
$(\mathbf{E}: Lagrangestrain, \mathbf{S}: secondPiola--Kirchhoffstress),$
$(\mathbf{L}: Henckystrain, \boldsymbol{\tau}: Kirchhoffstress)].$

To model the second-order stress–strain fields required for characterization of hyperelastic material, current approaches ranging from phenomenological to data-driven, face one major challenge, namely lack of data on 3D structures. There are no tools to measure stress field across a structure, and for strain, we can only measure the strain field for relatively simple structures using digital image correlation (DIC) techniques. The problem of considerable missing data has traditionally been solved by incorporating material behavior information into the model and constraining the model in advance of obtaining the data. Due to the lack of infused knowledge of the material, such a solution is irrelevant in data-driven approaches.

We propose to resolve the problem of significant missing data in finite deformation constitutive behavior through a physics-driven order-reduction approach by implementing the micro-sphere concept, network decomposition theory, continuum mechanics compatibility equations, and general rules provided by polymer physics on matrix behavior. Therefore, we will create a micro-mechanical model with super-constrained deep-learned agents serving as the constitutive models at 1D to predict the matrix behavior solely based on the macro-scale collective behavior of the sample. We have previously discussed [59,61] the formation of such algorithm for mechanical induced deformation as shown in Fig. 4. In other words, we will use exactly the same procedure of knowledge implementation into the model from our recent work, and the only difference is the network architecture used to define L-agents which is based on a new generation of machine learning algorithms known as conditional neural networks (CondNNs).

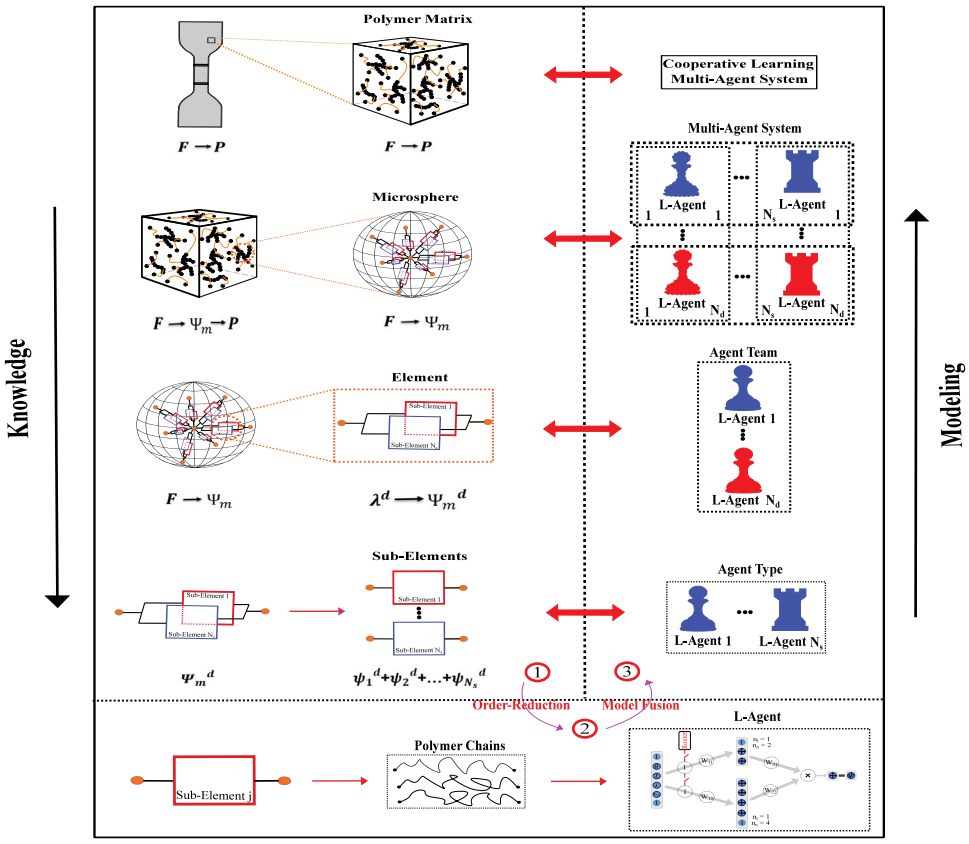

Fig. 4. Schematic of the proposed model from order-reduction to model fusion. It shows how we use the concepts from continuum mechanics, polymer sciences, physics, and machine learning to reduce the order of problem.

– ***Continuum mechanics.*** Using strain energy Ψ_m as the middle agent in stress–strain mapping, where $\mathbf{F} \rightarrow \Psi_m \rightarrow \mathbf{P}$, we replace the fourth-order mapping tensor with a scalar-valued function $\Psi_m(\mathbf{F})$. Strain energy can be portrayed with respect to any stress–strain work conjugates such as (i) two-point tensors, (ii) material tensors, or (iii) spatial tensors, as shown below

$$\mathbf{P} = \frac{\partial \Psi_m}{\partial \mathbf{F}}, \qquad \mathbf{S} = \frac{\partial \Psi_m}{\partial \mathbf{E}}, \qquad \boldsymbol{\tau} = \frac{\partial \Psi_m}{\partial \mathbf{L}}. \tag{3}$$

One specific benefit of using Ψ_m as the middle agent is that it guarantees the material objectivity and thermodynamic consistency on all the derived constitutive models (see Truesdell et al. [83]). There are several conditions on strain energy, which must be authorized in the data-driven model, to be specific

$$\begin{aligned} &\Psi_m(\mathbf{F}) \geq 0 \qquad when \quad \mathbf{F} \neq 0 \qquad Increase energy by deforming,\\ &\Psi_m(\mathbf{F}) = 0 \qquad when \quad \mathbf{F} = \mathbf{I} \qquad Normalization condition,\\ &\Psi_m(\mathbf{F}) \rightarrow \infty \qquad when \quad det\mathbf{F} \rightarrow \infty / 0 \qquad Growth condition. \end{aligned} \tag{4}$$

Meanwhile, ellipticity constraint is a significant challenge for hyperelastic materials. In the absence of traction forces, it can be applied by using strain energy.

– ***3D- To 1D transition: Microsphere.*** In virgin matrix, polymer chains are considered uniformly distributed in all spatial directions which implies matrix isotropy. Thus, by hiring the microsphere concept, we represent the 3D matrix as a homogeneous superassembly of multiple 1D elements spread over a microsphere in all spatial directions. Thus, the energy of the sphere is simply obtained by integrating over the energies of all elements, $\Psi_m = \frac{1}{4\pi}\int_S \Psi_m^{\boldsymbol{d}} dS^{\boldsymbol{d}}$. This methodology can help transferring knowledge from super-simplified 1D components to create a complex 3D polymer matrix. Furthermore, by discretizing the sphere into finite sections, the surface integration can be taken out numerically over N_d integration directions $[\boldsymbol{d}_i]_{i=1\ldots N_d}$ with various weight factors $[w_i]_{i=1\ldots n}$ [84]. The strain energy of polymer matrix Ψ_m in relation to its elements can therefore be written as

$$\Psi_m = \frac{1}{4\pi}\int_S \Psi_m^{\boldsymbol{d}} dS^{\boldsymbol{d}} \cong \sum_{i=1}^{N_d} w_i \Psi_m^{\boldsymbol{d}_i}, \qquad where \qquad \Psi_m^{\boldsymbol{d}_i} = \mathcal{B}^{\boldsymbol{d}_i} \tag{5}$$

where $\Psi_m^{\boldsymbol{d}_i}$ is the element energy in direction $\boldsymbol{d}_i$ which is represented by a team of L-agents $\mathcal{B}^{\boldsymbol{d}_i}$ reflecting an additive cooperation between multiple L-agents $\mathcal{B}^{\boldsymbol{d}_i} = \sum_{j=1}^{N_s} \mathcal{A}_j^i$ based on microsphere concept (see [84, 85]). To satisfy initial isotropy, we assume all teams to be identical in the virgin state, namely $\mathcal{B}^{\boldsymbol{d}_i} = \mathcal{B}^{\boldsymbol{d}_j}$. On the same note, during matrix deformation, different teams will be exposed to different deformations based on their directions, and the matrix becomes anisotropic. Consequently, the model can describe the directional onset of damage, deterioration, and propagation of cascading failure in anisotropic materials.

– ***Network decomposition.*** Network decomposition constraint is derived from statistical mechanics, namely by infusing the concept of superposition, which allows us to predict complicated patterns by superposing simple patterns on top of each other. To account for damage accumulation, the cross-linked matrix is hypothetically divided into a number of parallel networks, where each network represents one damage model. Accordingly, the entropic energy of the polymer matrix is the summation of the energies of the parallel networks. The platform is defined as a generalized set of assumptions to describe the micro-structure evolution through the mechanics of a single chain. The quasi-static deformation in polymeric joints are often induced by manufacturing process, thermal expansion and/or the coefficient of thermal expansion (CTE) mismatch between adhesive and adhered. The energy of the polymer matrix in the quasi-static deformation can

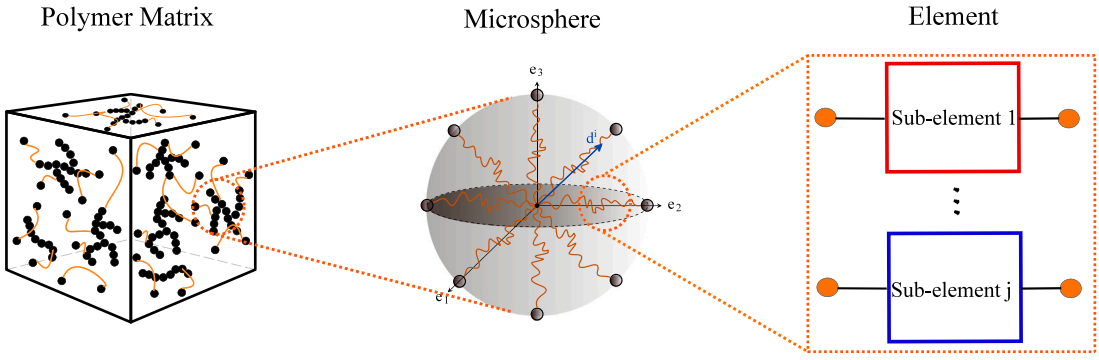

Fig. 5. The 3D- to 1D transition: Microsphere [86]. The orientation unit vector $\boldsymbol{d}$ can be parametrized by the spherical angles. The proposed numerical implementation uses 21 integration points with cartesian coordinates defined in Table C.1.

be given as the superposition of the energy of two parallel networks, which consist of polymers between crosslinks or between particles, respectively. Motivated by breakage of shorter chains during elongation and its consequent network rearrangement, *directional pre-stretch* will be used as a history variable to describe permanent damages, i.e., stress softening and permanent set.

Networks and subnetworks. Each network is considered to have a unique composition and describes a different energy-dissipating damage mechanism. Using the concept of micro-sphere, each network is considered as a 3D composition of infinite 1D subnetworks that are distributed in all spatial directions. Subnetworks can only be subjected to uniaxial deformation and thus will experience different deformations based on their directions. To develop a model for the subnetwork in direction, only a simplified form of entropic energy is needed with respect to uniaxial deformation. Integrating a subnetwork in all directions, the consequent network is a representation of that concept in a 3D configuration. The similar concept will be used for training of the neural network.

As a result, network decomposition helps us describing the complex behavior of a 1D element as the super-position of the simple behavior of N_s sub-elements, where $\Psi_m{}^{\boldsymbol{d}_i} = \sum_{j=1}^{N_s} \Psi_j{}^{\boldsymbol{d}_i}$. Here, each sub-element is responsible for one or no inelastic behavior. Assigning L-agent to each sub-element, $\mathcal{A}_j^i := \Psi_j{}^{\boldsymbol{d}_i}$, an element behavior is described by a team of cooperative L-agents $\mathcal{B}^{\boldsymbol{d}_i} = \sum_{j=1}^{N_s} \mathcal{A}_j^i$. Consequently, by substituting Eq. (5), we can extract the energy of the matrix directly with regard to sub-elements and the L-agents as

$$\Psi_m = \frac{1}{4\pi} \int_S \Psi_m{}^{\boldsymbol{d}} \, dS^{\boldsymbol{d}} \cong \sum_{i=1}^{N_d} \sum_{j=1}^{N_s} w_i \psi_j{}^{\boldsymbol{d}_i} := \sum_{i=1}^{N_d} \sum_{j=1}^{N_s} w_i \mathcal{A}_j^i. \tag{6}$$

Considering each sub-element is represented by an L-agent, the super-simplified scalar-to-scalar mapping behavior of a sub-element can be modeled by a simplified feed-forward neural network. Summarizing the implemented constraints, the first Piola–Kirchhoff stress tensor $\mathbf{P}$ can be derived on the basis of Eqs. (3) and (6), as

$$\mathbf{P} = \frac{\partial \Psi_m}{\partial \mathbf{F}} - p\mathbf{F}^{-T} := \sum_{i=1}^{N_d} \sum_{j=1}^{N_s} w_i \frac{\partial \mathcal{A}_j^i}{\partial \mathbf{F}} - p\mathbf{F}^{-T}, \tag{7}$$

where p signifies the Lagrange multiplier to ensure incompressibility of the material.

3.2. Conditional neural network (CondNN) L-agent

There is a new family of hybrid machine learning algorithms known as conditional neural networks (CondNNs) for problems in which the outputs are not only dependent on past occurrences, e.g., deformation effects on the matrix, but also on external actions, e.g., temperature and time of aging effects on the polymer matrix. This new algorithm has been derived by the combination of general neural network and decision tree concepts (see [87,88]). A routed behavior is a feature of decision trees; the data is sent to one or more children based on some learned routing function. This conditional computation means that we can infuse the knowledge in the model. Meanwhile, throughout many tasks, NNs achieve industry-leading precision for learning, but decision trees have the ability to infuse the knowledge into NNs. In other words, CondNNs are decision trees with the exception that instead of moving the data as is, each node applies a non-linear transformation to it. We can also forward the data to one or more of its children using routers.

In order to design an L-agent which can model mechanical and environmental damage in the polymer matrix, we use CondNNs as a new hybrid framework. The feed-forward L-agents consist of NNs followed by a fully connected layers, which the first branch represents the mechanical damage in the polymer matrix. The resulting features are then combined multiplicatively with the second branch of NN followed by fully connected layer that represents environmental damage in the matrix. (see Fig. 7)

– *Neural network architecture.* The architecture of the neural network (Fig. 7) is determined via the hyper-parameters summary: (i) number of hidden layers, n_l (network depth), (ii) number of neurons per hidden layers, n_n (network width), (iii) activation function.

Activation function : The activation function of a node in artificial neural networks determines the output of that node given input or a set of inputs. This is similar to the linear perceptron's behavior in neural networks. However, only nonlinear activation functions allow such networks, using only a small number of nodes, to measure non-trivial problems, and such activation functions are called non-linearities. Choosing the activation function has a significant impact on the neural network's capacity and efficiency, and various activation functions can be used in different sections of the model. Based on the type of neural network architecture, the activation function used in hidden layers is usually chosen. If we are unsure which activation function to use for our network, we try and compare the results to find the best ones. We have done the same procedure in this study. Note that the choice of activation function in the hidden layer will control how well the network model learns the training dataset. Also, the effect of choosing different activation functions has not a significant effect on training time [89]. (See Figs. 5 and 6.)

For training of the described problem, it is crucial to use activation functions tailored to the underlying physical output quantities. Using physics-based rationale, an activation function with a positive output parameter for tension and a negative output parameter for compression and non-zero derivative (which is important in physics-based neural networks) is an obvious choice. For all hidden layers, the hyperbolic tangent function is used, which is a preferable activation function due to its smoothness and non-zero derivative.

Note that Rectified Linear Unit activation function or ReLU for short is a piecewise linear function that will output the input directly if it is positive, otherwise, it will output zero. Also, The Exponential Linear

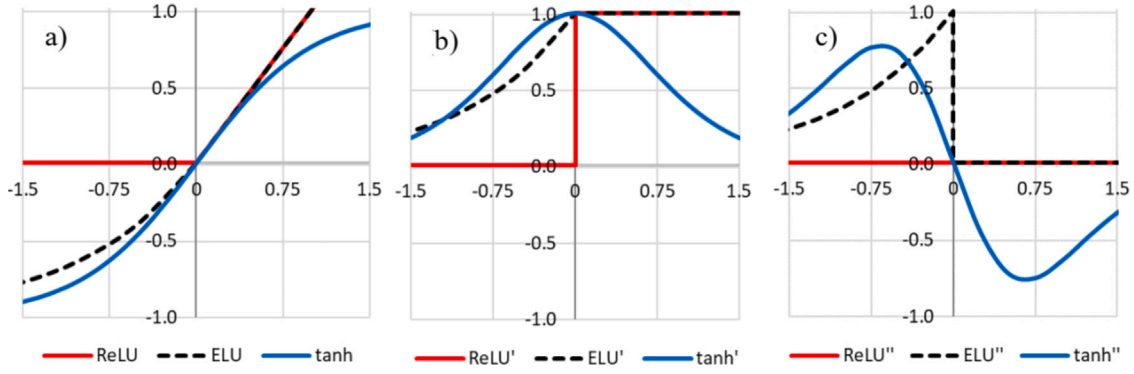

Fig. 6. (a) ReLU (Rectified Linear Unit), ELU (Exponential Linear Unit) and tanh activation functions, (b) first derivatives of activation functions, and (c) second derivatives of activation functions [90].

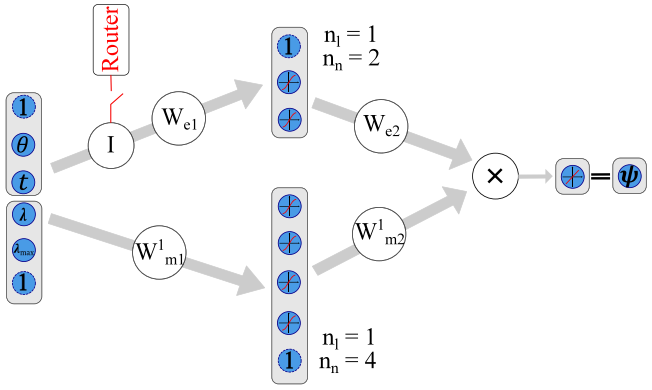

Fig. 7. Schematic of a neural network with physics-informed engineered features to learn the effect of environmental aging on the mechanical Behavior. This is referred to as CNN in this study.

Unit (ELU) is an activation function for neural networks. In contrast to ReLUs, ELUs have negative values which allows them to push mean unit activation closer to zero.

The L-agent response is computed using a feed-forward algorithm for a given set of hyper-parameters (n_l, n_n). Each L-agent can be represented by a CondNNs as

$$\mathcal{A}^i_j := \mathcal{D}^{d_i}(\boldsymbol{E}^i)\psi^{d_i}_j(\boldsymbol{M}_j{}^i, \boldsymbol{S}_j{}^i) \qquad \mathcal{D}^{d_i} = CNN_e(\mathbf{W_e}, \boldsymbol{E}^i),$$
$$\psi^{d_i}_j = CNN_m(\mathbf{W^j_m}, \mathbf{M_j}^i, \mathbf{S_j}^i), \tag{8}$$

where $\psi^{d_i}_j$ represents the energy of deformation-induced damage part and $\mathcal{D}^{d_i}$ is related to environmental damage of one sub-element. Similarly, two weight matrices $\mathbf{W_m}^j = \left[\boldsymbol{W}_{m^j_1} \ldots \boldsymbol{W}_{m^j_{n_l+1}}\right]$ and $\mathbf{W_e} = \left[\boldsymbol{W}_{e1} \ldots \boldsymbol{W}_{e_{n_{l+1}}}\right]$ are related to weight matrices of mechanical and environmental damage CondNNs, respectively. Here, $\psi^i_j(\boldsymbol{M}_j{}^i, \boldsymbol{S}_j{}^i)$ is trained on the basis of a non-kinematic input sets $\boldsymbol{M}_j{}^i$ and internal parameters $\boldsymbol{S}_j{}^i$ for the mechanical damage CondNN. Selection of internal parameters depend on (full or recent) material memory. Also, the input vector $\boldsymbol{E}^i$ should represent the setting of the problem related to environmental damage such as temperature and time of degradation.

Normalization, conditions of growth, isotropy, objectivity, and polyconvexity are already satisfied in the proposed equation (Appendix).

– ***Model parameter identification.*** The parameters of the CondNN model are identified using a Gradient descent algorithm. A data collection consisting of n data points is the basis for model recognition. Loss function was defined with respect to the difference between target values, AKA experimental data, and approximated value, AKA CondNN output. Here, we define the loss function $\mathcal{L}$ Mean Squared Error (MSE) for a total of n_{tot} data points as

$$\mathcal{L}(\mathbf{W^1_m}, \ldots., \mathbf{W^j_m}, \mathbf{W_e}) = \frac{1}{2}\sum_{n=1}^{n_{tot}}\left[\boldsymbol{g}_1\left(\sum_{i=1}^{N_d}\sum_{j=1}^{N_s} w_i \frac{\partial \mathcal{A}^i_j}{\partial \mathbf{F}} - p\mathbf{F}^{-T}\right)\boldsymbol{g}_1 - P^{11}_n\right]^2, \tag{9}$$

where $P^{11}_n := \boldsymbol{g}_1\mathbf{P}\boldsymbol{g}_1$ is the first component of the experimental macroscale stress tensor $\mathbf{P}_n$ in loading direction $\boldsymbol{g}_1$ for point n.

4. Validation: Environmental + mechanical damages in rubber

Here, the proposed hybrid model is developed and validated for two different loading scenarios

1. Thermal-induced aging + Mechanical deformation (Mullins effect)
2. Hydrolysis (desalinated water) + Mechanical deformation (Mullins effect)

In both cases, the model was benchmarked against experimental data to predict the inelastic behavior of cross-linked elastomers for different states of deformation at different stages of aging. We also validated the model predictions for different coupling scenarios for mechanical and environmental damages, namely

– **Intermittent test** where the sample has been aged first with no stress, and then the mechanical behavior is characterized

– **Relaxation test** where the samples were loaded and aged at constant deformation and the drop in the stress has been recorded.

In both cases, the predictions were validated against four main variables the effect of (i) deformation, (ii) deformation history, (iii) aging time (t), and (iv) aging temperature (θ).

4.1. Network architecture

For modeling both loading scenarios, we used identical engines; a relatively simple engine built by $N_d = 21$ teams, where each team had $N_s = 2$ agents [84]. Note that the number of teams and their related agents can be chosen based on the trade-off between accuracy and computational cost. In other words, we consider 21 teams because it is a small number for estimation of the integral with a summation. As a result, it guarantees that the proposed model error in prediction is excellent even in a small number of teams. To capture all deformation states, we used only two agents, each of which is representative of the first and second invariants of the Green-Cauchy deformation tensor. For the CondNNs structure of L-agents, we considered one input layer, one hidden layer with four neurons and three activation functions soft plus $\psi(\bullet) = ln(1 + e^{\bullet})$, sinusoid $\psi(\bullet) = sin(\bullet)$ and hyperbolic tangent $\psi(\bullet) = tanh(\bullet)$.

The internal parameters of L-agents were built via λ_{j-max} parameters to capture the deformation of the rubbers with full memory. In order to allow teams to predict various deformation states, the first and

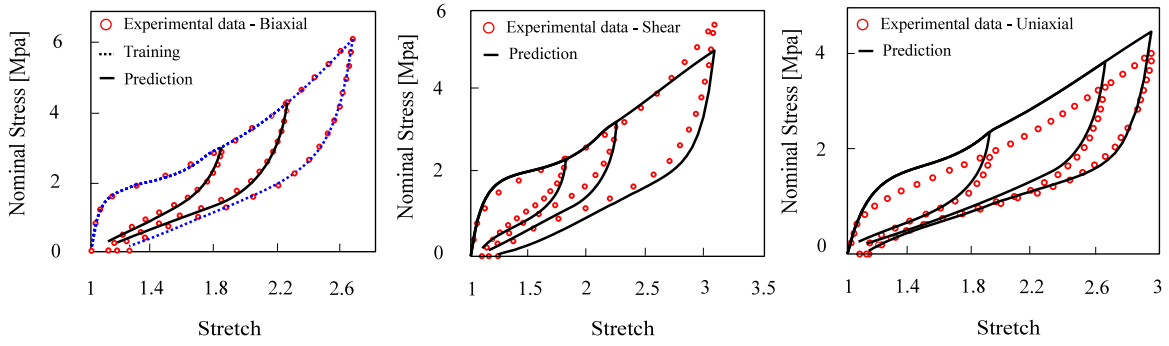

Fig. 8. Model training and prediction of bi-axial, pure shear, and uni-axial(Urayama's dataset [91]). Dash lines stand for fitting and solid lines stand for prediction. The biaxial dataset which have been showed with the blue line used for training and of the model. The black lines in bi-axial, shear, and uni-axial datasets show the performance of the model in prediction after training.

second deformation invariants were supplied to each team [92,93]. The condition was satisfied by providing input sets into the first and second L-agents as

$$\begin{aligned} &\boldsymbol{M}_1^{d_i} = [\lambda^{\boldsymbol{d_i}}], \quad \boldsymbol{S}_1^{d_i} = [\lambda_{max}^{\boldsymbol{d_i}}], \quad \boldsymbol{E}^{d_i} = [t, \theta], \quad \boldsymbol{M}_2^{d_i} = [\nu^{\boldsymbol{d_i}}], \\ &\boldsymbol{S}_2^{d_i} = [\nu_{max}^{\boldsymbol{d_i}}], \quad \boldsymbol{E}^{d_i} = [t, \theta], \end{aligned} \tag{10}$$

while

$$\lambda^{\boldsymbol{d_i}} = \sqrt{\boldsymbol{d_i C d_i}}, \qquad \nu^{\boldsymbol{d_i}} = \sqrt{\boldsymbol{d_i} \mathbf{C}^{-1} \boldsymbol{d_i}}, \qquad \mathbf{C} = \mathbf{F}^T \mathbf{F} \tag{11}$$

where $\left[\boldsymbol{d}_i\right]_{i=1\ldots N_d}$ is integration directions in micro-sphere, $\lambda^{\boldsymbol{d_i}}$ and $\nu^{\boldsymbol{d_i}}$ are related to I_1 and I_2, as the first and second invariants of $\mathbf{C}$, respectively.

In summary, the rubber matrix was represented by a cooperative game of 21 teams of 2 agents through $\mathcal{A}_j^i$, $i \in \{1, 21\}$, $j \in \{1, 2\}$. After agent fusion, the final cost function is given by

$$\mathcal{L}(\mathbf{W}_m^1, \mathbf{W}_m^2, \mathbf{W}_e) = \frac{1}{2} \sum_{n=1} [\boldsymbol{g}_1 (\sum_{i=1}^{21} \sum_{j=1}^{2} w_i \frac{\partial \mathcal{A}_j^i}{\partial \lambda_j^{\boldsymbol{d}_i}} \frac{\partial \lambda_j^{\boldsymbol{d}_i}}{\partial \mathbf{F}} - p\mathbf{F}^{-T}) \boldsymbol{g}_1 - P_n^{11}]^2, \tag{12}$$

subjected to weights related to λ_{max} and $\nu_{max} \leqslant 0$, and weights related to λ and $\nu \geqslant 0$ to satisfy thermodynamic consistency and polyconvexity, respectively. Accordingly, the energy of each sub-element can be written with respect to the deformation gradient $\mathbf{F}$ as follows

$$\sum_{i=1}^{21} w_i \frac{\partial \mathcal{A}_1^i}{\partial \lambda^{\boldsymbol{d}_i}} \frac{\partial \lambda^{\boldsymbol{d}_i}}{\partial \mathbf{F}} = \sum_{i=1}^{21} w_i \frac{\partial \mathcal{A}_1^i}{\partial \lambda^{\boldsymbol{d}_i}} \frac{1}{\lambda^{\boldsymbol{d}_i}} \mathbf{F} \left(\boldsymbol{d}_i \otimes \boldsymbol{d}_i\right). \tag{13}$$

$$\sum_{i=1}^{21} w_i \frac{\partial \mathcal{A}_2^i}{\partial \nu^{\boldsymbol{d}_i}} \frac{\partial \nu^{\boldsymbol{d}_i}}{\partial \mathbf{F}} = -\sum_{i=1}^{21} w_i \frac{\partial \mathcal{A}_2^i}{\partial \nu^{\boldsymbol{d}_i}} \frac{1}{\nu^{\boldsymbol{d}_i}} \mathbf{F}^{-1} \mathbf{F}^{-T} \mathbf{F}^{-1} \left(\boldsymbol{d}_i \otimes \boldsymbol{d}_i\right). \tag{14}$$

Minimizing data requirement for training. For history-dependent materials, parameters should be specifically chosen to represent material's damage and then fed into the L-agents through internal parameters. However, different types of damage parameters may be required for describing different materials, e.g., for materials with recent memory such as visco-elastic materials, internal parameters should transfer information from each iteration to the next. In contrast, for materials with full memory such as elastomers, the internal parameters can be defined independently of the solution iterations as a damage-precursor of the external events; for example, the maximum stretch and aging time/temperature in rubber material can be used as a damage precursor to show the history of damage in each direction. So, each L-agents in all directions consists of damage parameters.

The reason for training with biaxial datasets roots from the point that we cannot train agents with scenarios in which they are not involved or have a minor role to play. As a result, the quality of the training data and the contribution of agents in those situations are strongly proportional to the confidence in agent training. We can measure the confidence interval in which an agent may be trained with high confidence with regard to the provided data by describing the quality of data with respect to the input required by each agent. Too little data can give us a false sense of safety because it prevents us from seeing the crucial points, while low-quality data can lead to incorrect conclusions that appear to be completely reliable. We added two L-agent types in the aforementioned rubber model, which represent two sub-elements using $\boldsymbol{M}_1^{d_i}$ and $\boldsymbol{M}_2^{d_i}$ input sets, respectively. We know from the definition of $\boldsymbol{M}_2^{d_i}$ that it has a restricted variation in uni-axial tensile stress; therefore, the contribution of the second L-agent in such loading is essentially non-existent. However, because $\boldsymbol{M}_2^{d_i}$ changes greatly in bi-axial stress, the contribution of the second L-agent is fairly important in this instance. Because the second agent cannot be completely engaged, training using uniaxial data cannot give the quality information required for reliable training of both agents (please see our recent paper [59]). The reason for training with different states of deformation is that we want to show the performance of the model by choosing different datasets. If we train the model based on uniaxial tensile data till stretch χ_x, the model can predict different states of deformation based on the ranges that the model has calibrated based on that. In order to ensure accurate prediction of the model, the prediction ranges should be in the range that the agent is trained. Thus, in the bi-axial prediction case, the model is limited to

$$\begin{aligned} &Agent1: \quad \left[\frac{1}{\chi_{bi.}^2}, \chi_{bi.}\right] \in \left[\frac{1}{\sqrt{\chi_x}}, \chi_x\right] \longrightarrow \chi_{bi.} \leq \sqrt[4]{\chi_x} \\ &Agent2: \quad \left[\frac{1}{\chi_{bi.}}, \chi_{bi.}^2\right] \in \left[\frac{1}{\chi_x}, \sqrt{\chi_x}\right] \longrightarrow \chi_{bi.} \leq \sqrt[4]{\chi_x}. \end{aligned} \tag{15}$$

4.2. Step 1: CondNN training in the absence of aging

To investigate the performance of the proposed model in the material in the absence of aging, we benchmarked the inelastic features in the behavior of natural rubber, namely Mullins effect and permanent set. Figure 8 shows stress–stretch curves for this cross-linked polymer with experimental data of [91]. We used one set of bi-axial loading-unloading until $\lambda = 2.7$ for training and predicting inelastic effects in different states of deformation, e.g., uniaxial and pure shear at increasing stretch amplitudes which constitutes deformation histories.

4.3. Case study 1: Thermo-oxidation + mechanical damage

Natural rubber. Prediction of aging was validated against experiments for samples aged at various times and temperatures. Firstly, experimental data from natural rubber relaxation test filled with 60 phr carbon-black was used to demonstrate model results (see Fig. 9). Intermittent test results were also used to verify the model's functionality to predict the impact of various degrees of aging alongside various strains (see Fig. 10). The training dataset is chosen to cover different relaxation stretches and the highest and lowest effect of temperature and time in order to increase the predictability of the model for different temperatures and times. Note that the model is just able to capture the relation effect of aging, not the relaxation effect of viscosity.

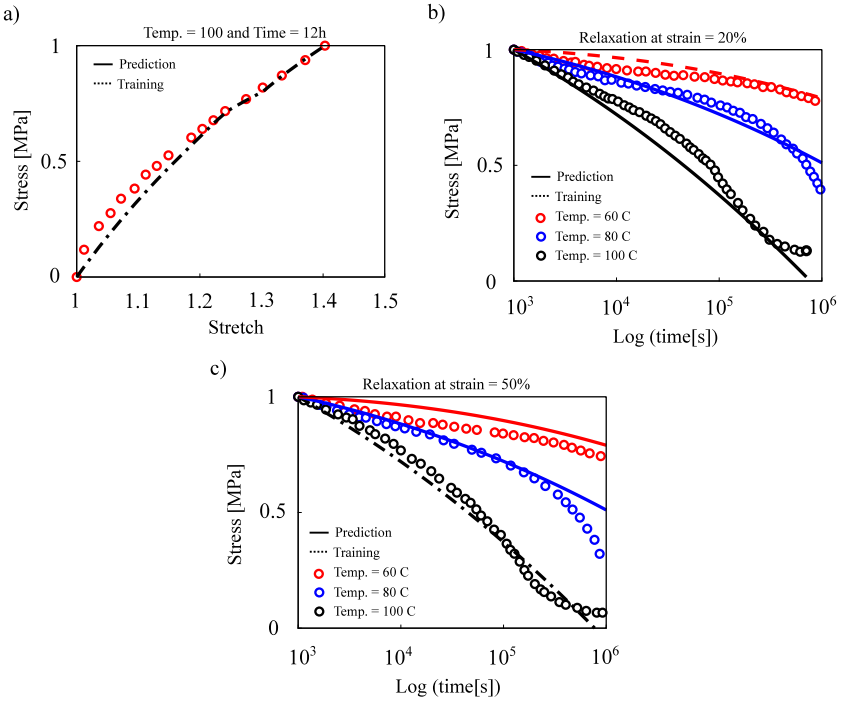

Fig. 9. Training and model predictions for NR against; (a) intermittent test, (b) relaxation test at $\epsilon = 20\%$, (c) relaxation test at $\epsilon = 50\%$. Dash lines stand for fitting and solid lines stand for prediction. The red points in figure (a) and (b), and the black points in the figure (c) have been used for training of the model. The solid lines show the performance of the model in prediction after training.

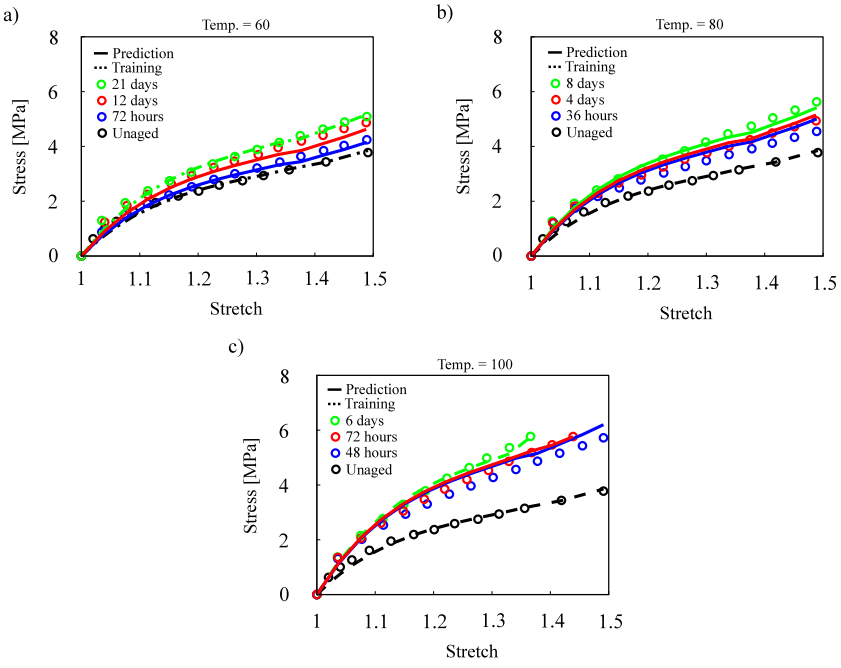

Fig. 10. Training and model predictions for NR against intermittent test; (a) at 60 °C, (b) at 80 °C, (c) at 100 °C. Dash lines stand for fitting and solid lines stand for prediction. The black(unaged) and green points in the figure (a) and (c), and just the black(unaged) points in figure (b) have been used for training. The solid lines show the performance of model in prediction after the training.

Polyurethane. A bone form punch was used to punch dumbbell samples in compliance with ASTM D412 standards. The reason that we are using dog-bone samples is that in this shape, when we put the extensometer in a specific location of that sample, we are sure that it gives us one component of the deformation matrix, for example, x-x direction. But in complex shapes, several components of stress tensor participate; so, it is not possible to see the effect of each component with an external extensometer. Three different temperatures, 60 °C, 80 °C, and 95 °C, in zero humidity level, were used to age the samples. The performance of the invented model was determined using the results of the uni-axial tensile failure tests. Fig. 11 depicts the evaluation's related findings.

Silicon adhesive. To assess the model's capabilities, we compared its predictions to our experimental results, which were specifically developed to demonstrate the effect of chemical aging on the constitutive response of silicone adhesive. In this case, samples were placed in ovens

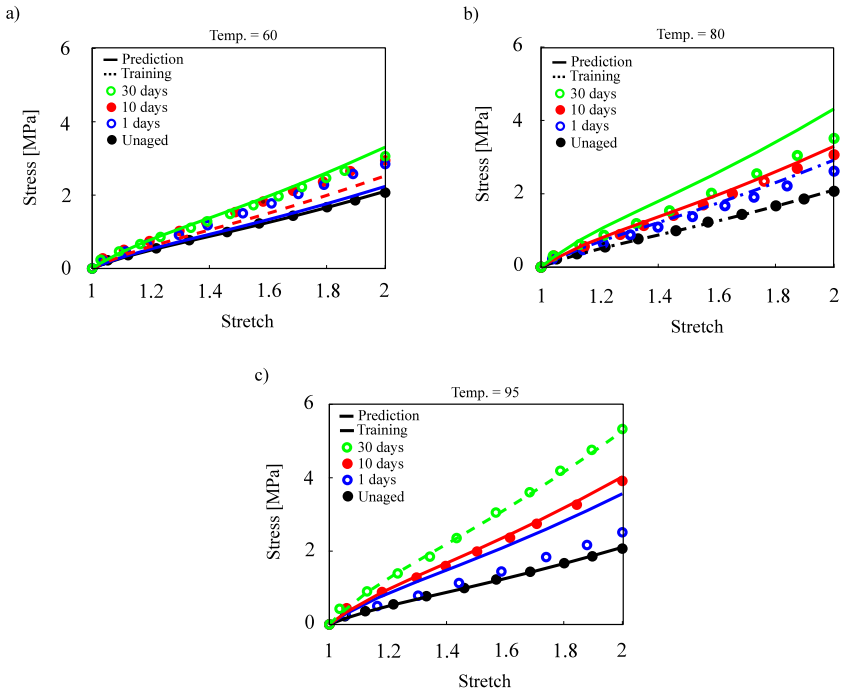

Fig. 11. Training and model predictions for polyurethane against intermittent test; (a) at 60 °C, (b) at 80 °C, (c) at 95 °C. Dash lines stand for fitting and solid lines stand for prediction. The black(unaged) and red points in the figure (a), the black(unaged) and blue points in figure (b), and the black(unaged) and green points in the figure (c) have been used for training. The solid lines show the performance of model in prediction after the training.

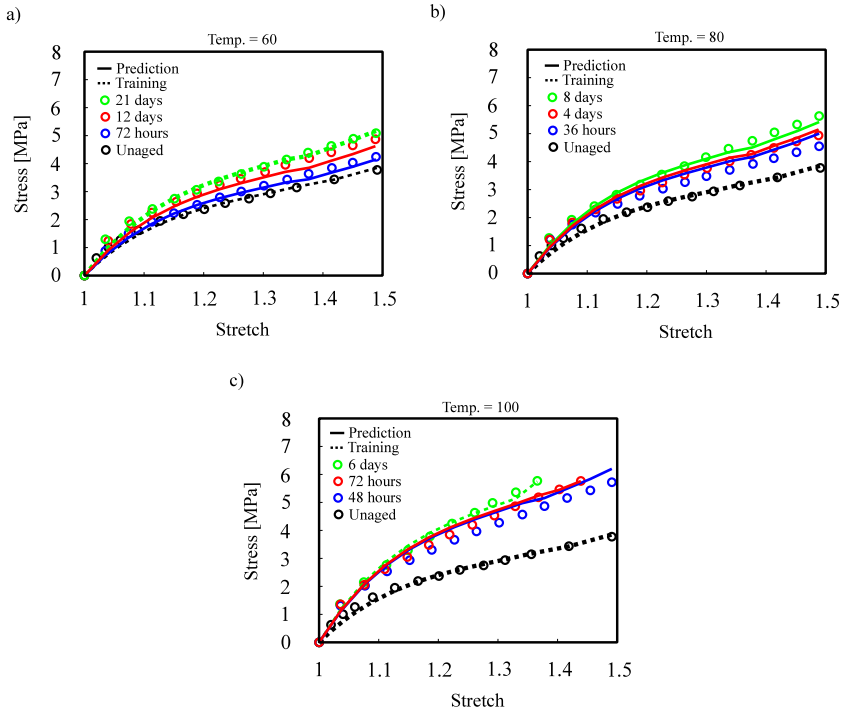

Fig. 12. Training and model predictions for silicone adhesive against intermittent test; (a) at 60 °C, (b) at 80 °C, (c) at 100 °C. Dash lines stand for fitting and solid lines stand for prediction. The black(unaged) and green points in the figure (a), the black(unaged) points in figure (b), and the black(unaged) and green points in the figure (c) have been used for training. The solid lines show the performance of model in prediction after the training.

at temperatures 60 °C, 80 °C, and 100 °C with a relative humidity of zero (i.e. RH= 0%). All of the specimens were aged under constant pressure, and after a set amount of time, they were removed from the containers and dried with tissue paper. The predictions of the proposed model against the experimental data for different types of aging and different amount of aging times, temperatures, and deformations are plotted in figure 12.

Note that the model is able to predict the behavior of elastomers even in the stretch greater than 4. Thermo-oxidative aging makes the samples brittle. As a result, the failure point for samples happens on

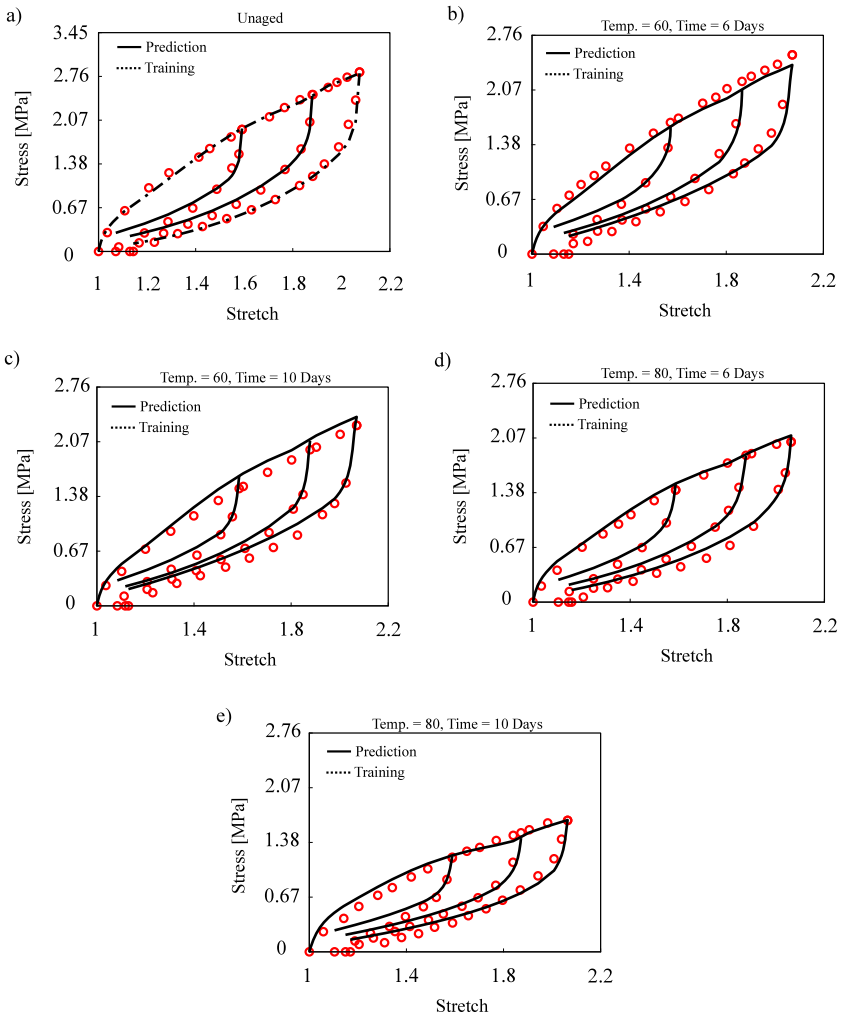

Fig. 13. Multiple SBR training and model predictions; (a) unaged, (b) constitutive behavior for 6 days of age at temperature study of 60 °C, (c) constitutive behavior for 10 days of age at temperature study of 60 °C, (d) constitutive behavior for 6 days of age at temperature study of 80 °C, (e) constitutive behavior for 10 days of age at temperature study of 80 °C. Dash lines stand for fitting and solid lines stand for prediction.

the less stretch. So, because the focus of the proposed model is on the behavior of aged materials we showed the performance of the model till stretch less than 4. In addition, the kernel of model is the same even for higher stretches. So, the model works for higher stretch as well.

4.4. Case study 2: Hydrolysis + mechanical damage

Styrene-butadiene rubber (SBR). samples were placed at temperatures of 60 °C and 80 °C at 1 bar pressure in sealed containers filled with distilled water. After aging, samples were removed and dried at room temperature for ten days. We used an SFM-20 united testing machine with a 1000 lb load cell for quasi-static tensile tests. A strain rate of $43.29\frac{\%}{min}$ was used at room temperature for extension. The samples were subjected to uni-axial tensile test to failure in monotonic failure experiments, but the samples were expanded to preset amplitudes of 1.3, 1.6, 1.9, and 2.1 in the cyclic test. The central zone extension was measured using an external extensometer. Fig. 13 shows the effect of time and temperature on damages induced by deformation.

Silicon adhesive. In sealed containers filled with distilled water, samples were held at 60 °C, 80 °C, 95 °C, and 1 bar pressure. After aging, samples were removed and dried for 1, 10, and 30 days at room temperature. For quasi-static tensile tests, we used an SFM-20 united testing system with a 1000 lb load cell. Fig. 14 depicts the influence of time and temperature on deformation-induced damage.

Other compounds. with behavior reported in the literature were also used for validation of the proposed model to predict behavior with complex patterns of inelasticity, such as hardening and curvature alteration. Here, we have been generalizing the experimental data available in the literature to form a model for predicting the hydrolytic aging activity of three other compounds. Fig. 15 shows the excellent performance of the devised model in prediction of mechanical behavior of Poly-Urethane submerged at 100 °C in seawater [94], PLA-PCL fiber at 37 °C submerged in phosphate buffer solution [70], Natural rubber (vulcanized A) submerged in seawater at 40 °C [95].

5. Conclusion

The aim of this paper was to propose a novel physics-informed hybrid framework to capture the relation between elastomeric network mechanics and environmental damage. The proposed model is used to describe the effect of single-mechanism aging, such as thermal-induced or hydrolytic aging, on the behavior of the material in this hybrid system. Huge chain scission, cross-link reduction, chain formations, and changes in polymer morphology are all examples of environmental single-mechanism damages that alter the polymer matrix over time. In other words, this model is a predictive model and not a descriptive model. As a result, it can provide prediction in a fraction of time and cost to the end-users for the reliable design of components. Although,

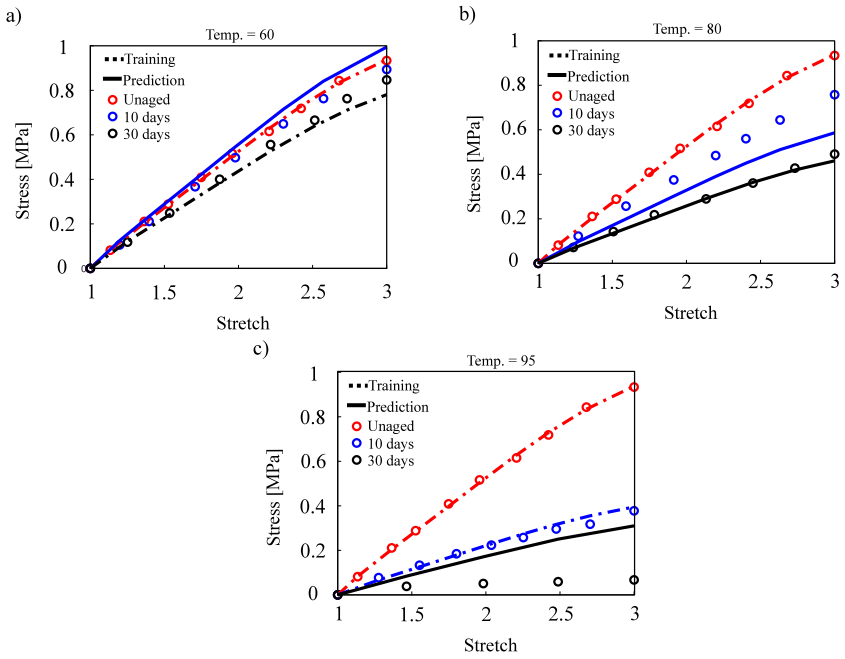

Fig. 14. Training and model predictions for silicon adhesive against intermittent test; (a) at 60 °C, (b) at 80 °C, (c) at 95 °C. Dash lines stand for fitting and solid lines stand for prediction. The red(unaged) and black points in the figure (a), the red(unaged) points in figure (b), and the red(unaged) and blue points in the figure (c) have been used for training. The solid lines show the performance of model in prediction after the training.

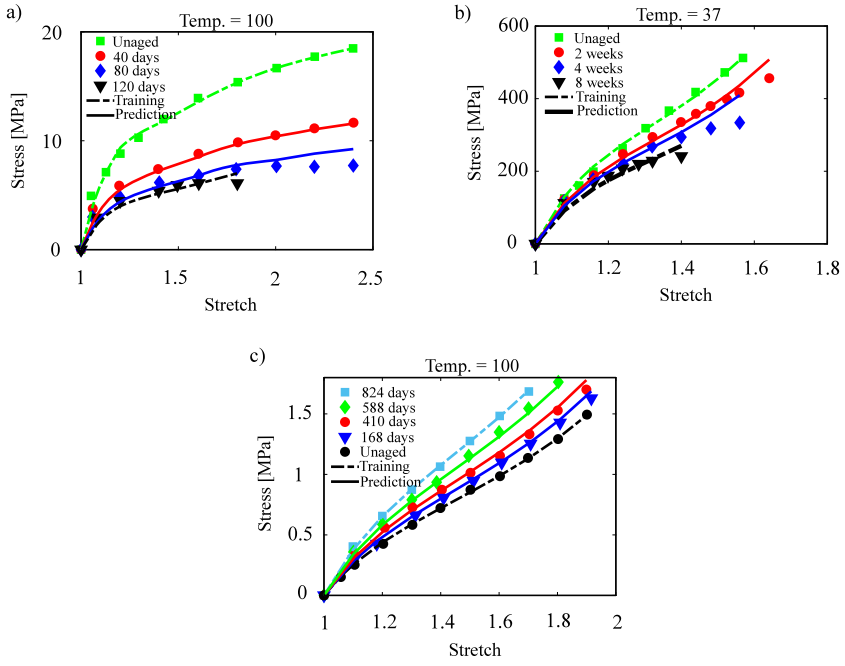

Fig. 15. Training and model predictions of three different materials against aging; (a) PolyUrethane (PU) submerged at 100 °C in seawater [94], (b) PLA-PCL fiber at 37 °C submerged in phosphate buffer solution [70], (c) Natural rubber (vulcanized A) submerged in seawater at 40 °C [95]. Dash lines stand for fitting and solid lines stand for prediction.

The model cannot be used to understand or explore kinetics. By extracting micro-structural activity from macroscopic experimental data, the data-driven approach aims to overcome the shortcomings of both phenomenological and micro-mechanical models.

The model arises from polymer physics and an order reduction strategy ending to the constrained L-agents training. The polymer matrix was described by a cooperative multi-agents system, in which each agent is represented by a simple deep-learned CondNN that is super-constrained by laws derived from physics, thermodynamics, and continuum mechanics. While satisfying the continuum mechanics and thermodynamics rules, the proposed hybrid model is quite simple for the most rubbery media in the extreme environment.

The excellent performance of the proposed method was proven by validating against different experimental data on different materials that are particularly selected to reveal the evolution of inelastic behavior during single mechanism agings. The efficiency of the model was found satisfactory, and in some cases, excellent when compared with the experimental data. “In general, the error of our model in training and prediction is less than 10%.” Accuracy and simplicity of the model make it a proper choice for commercial and industrial

Table C.1
Integration points and weighting factors of the unit-sphere.

i	$d_i(1)$	$d_i(2)$	$d_i(3)$	w_i
1	0.0	0.0	1.0	0.0265214244093
2	0.0	1.0	0.0	0.0265214244093
3	1.0	0.0	0.0	0.0265214244093
4	0.0	0.707106781187	0.707106781187	0.0199301476312
5	0.0	0.707106781187	0.707106781187	0.0199301476312
6	0.707106781187	0.0	0.707106781187	0.0199301476312
7	0.707106781187	0.0	0.707106781187	0.0199301476312
8	0.707106781187	0.707106781187	0.0	0.0199301476312
9	0.707106781187	0.707106781187	0.0	0.0199301476312
10	0.836095596749	0.387907304067	0.387907304067	0.0250712367487
11	0.836095596749	0.387907304067	0.387907304067	0.0250712367487
12	0.836095596749	0.387907304067	0.387907304067	0.0250712367487
13	0.836095596749	0.387907304067	0.387907304067	0.0250712367487
14	0.387907304067	0.836095596749	0.387907304067	0.0250712367487
15	0.387907304067	0.836095596749	0.387907304067	0.0250712367487
16	0.387907304067	0.836095596749	0.387907304067	0.0250712367487
17	0.387907304067	0.836095596749	0.387907304067	0.0250712367487
18	0.387907304067	0.387907304067	0.836095596749	0.0250712367487
19	0.387907304067	0.387907304067	0.836095596749	0.0250712367487
20	0.387907304067	0.387907304067	0.836095596749	0.0250712367487
21	0.387907304067	−0.387907304067	0.836095596749	0.0250712367487

application because we do not need to know the exact behavior and interaction of micro-structures; however, in the future, the model can be extended to consider viscoelasticity and non-isotropic formation for better precision due to platform of the model. Besides, note that the proposed model focus is on the mechanical behavior of the material during degradation, not lifetime prediction. Also, the performance of the proposed model is completely dependent on the dataset that we choose for training. It is axiomatic that if we increase the available dataset for training, the predictionability of the model is more accurate.

Declaration of competing interest

The authors declare that they have no known competing financial interests or personal relationships that could have appeared to influence the work reported in this paper.

Acknowledgment

The authors acknowledge partial financial support from the U.S. Department of Energy's Office of Energy Efficiency and Renewable Energy (EERE) under the Award Number DE-EE0008455.

Appendix A. Frame independency

Frame objectivity allows the material's strain energy to remain unchanged during rigid body motion. Therefore, the material reaction does not rely on the choice of frame of reference. The dependency of the strain energy frame can be written as

$$\Psi_m(\mathbf{QF}, t, \theta) = \Psi_m(\mathbf{F}, t, \theta), \tag{A.1}$$

Where $\mathbf{Q}$ is the tensor of rotation. So if energy is left rotationally invariant, a constitutive equation is frame-independent. Due to the property of right Cauchy–Green deformation tensor $\mathbf{C}$, if the strain energy is a function of the right Cauchy–Green deformation tensor $\mathbf{C}$, the specified condition is met.

$$\mathbf{C}^{+} = (\mathbf{F}^{+})^{T}\mathbf{F}^{+} = \mathbf{F}^{T}\mathbf{Q}^{T}\mathbf{QF} = \mathbf{F}^{T}\mathbf{F} = \mathbf{C}, \tag{A.2}$$

which $\mathbf{F}^{+} = \mathbf{FQ}$. The proposed model is a function of right Cauchy–Green deformation tensor. So the condition of frame independency is immediately fulfilled.

Appendix B. Thermodynamic consistency

B.1. Polyconvexity

Polyconvexity is one of the conditions considered to guarantee the stability of thermodynamics. We briefly define sufficient but not required free energy function conditions in this section that guarantee the existence of minimizers of certain variational principles. We begin with some properties of convexity to understand polyconvexity. Take into account that $\Psi m(\mathbf{F}, t, \theta)$ is a function of strain energy in the K set. We can say $\Psi_m(\mathbf{F}, t, \theta)$ is convex on set of K if hessian matrix of $\Psi_m(\mathbf{F}, t, \theta)$ be positive in that set.

$$D^2\Psi_m(\mathbf{F}, t, \theta).(H, H) \geqslant 0, \tag{B.1}$$

and we can note for proof of polyconvexity that $\mathbf{F} \rightarrow \Psi_m(\mathbf{F}, t, \theta)$ is polyconvex if and only if a G function exists such that

$$\Psi_m(\mathbf{F}, t, \theta) = G(\mathbf{F}, \mathrm{adj}\mathbf{F}, \det\mathbf{F}, t, \theta), \tag{B.2}$$

and the function G is convex. Besides, $\mathrm{adj}\mathbf{F} = \frac{\mathbf{F}^{-1}}{\det\mathbf{F}}$ and the implication chain shows relations from convexity to ellipticity.

convexity → polyconvexity → quasiconvexity → ellipticity

The Hessian matrix of the strain energy is positive if

$$\frac{\partial {\Psi_m}^2}{\partial^2 {\lambda_j}^{\boldsymbol{d}_i}} = \sum_{i=1}^{N_d} w_i \frac{\partial {\psi_j}^{\boldsymbol{d}_i 2}}{\partial^2 {\lambda_j}^{\boldsymbol{d}_i}} = \sum_{i=1}^{N_d} w_i \frac{\partial \mathcal{D}^j CNN_m(\mathbf{W_m}, {\lambda_j}^{\vec{d}_i}, {\lambda_j}_{max}^{\vec{d}_i})}{\partial {\lambda_j}^{\boldsymbol{d}_i}} > 0,$$
$$for\ j = 1, 2, \ldots, N_s, \tag{B.3}$$

If weights connecting the input of λj to other neurons are positive, the polyconvexity state is preserved by the proposed model.

B.2. Second law of thermodynamic

Since all constitutive models should satisfy the second thermodynamic equation, the proposed model should be tested for satisfaction with this equation. Checking Clausius–Duhem inequality, on the other hand, will be enough for this. Because $\lambda jmax$ are internal variables in the Cross-linked elastomers strain energy function, we may reduce the second thermodynamics equation to Clausius–Duhem inequality, which

shows the model's thermodynamic consistency in the direction di. This inequality can be written as

$$\frac{\partial \Psi_m}{\partial \lambda_{jmax}{}^{\boldsymbol{d}_i}} \leq 0, \qquad \frac{\partial \Psi_m}{\partial t} \leq 0, \qquad \frac{\partial \Psi_m}{\partial \theta} \leq 0, \qquad \forall\ \boldsymbol{d}$$
$$for\ j = 1, 2, \dots, N_s, \tag{B.4}$$

If we consider the energy of matrix as

$$\Psi_m = \sum_{i=1}^{N_d} \sum_{j=1}^{N_s} \left(\psi_j{}^{\boldsymbol{d}_i}\right) w_i, \tag{B.5}$$

which

$$\overset{\boldsymbol{d}}{\psi}_j = \mathcal{D}^j CNN_m(\mathbf{W_m}, \lambda_j{}^{\vec{d}_i}, \lambda_{j_{max}}{}^{\vec{d}_i}), \tag{B.6}$$

thus, Clausius–Duhem can be written as

$$\frac{\partial \Psi_m}{\partial \lambda_{j\,max}{}^{\boldsymbol{d}_i}} = \sum_{i=1}^{N_d} w_i \frac{\partial \psi_j{}^{\boldsymbol{d}_i}}{\partial \lambda_{j\,max}{}^{\boldsymbol{d}_i}} = \sum_{i=1}^{N_d} w_i \frac{\partial \mathcal{D}^j CNN_m(\mathbf{W_m}, \lambda_j{}^{\vec{d}_i}, \lambda_{j\,max}{}^{\vec{d}_i})}{\partial \lambda_{j\,max}{}^{\boldsymbol{d}_i}} \leq 0,$$
$$for\ j = 1, 2, \dots, N_s, \tag{B.7}$$

$$\frac{\partial \Psi_m}{\partial t} = \sum_{i=1}^{N_d} w_i \frac{\partial \psi_j{}^{\boldsymbol{d}_i}}{\partial t} = \sum_{i=1}^{N_d} w_i \frac{\partial \mathcal{D}^j CNN_m(\mathbf{W_j}, \lambda_j{}^{\vec{d}_i}, \lambda_{j\,max}{}^{\vec{d}_i})}{\partial t} \leq 0,$$
$$for\ j = 1, 2, \dots, N_s, \tag{B.8}$$

$$\frac{\partial \Psi_m}{\partial \theta} = \sum_{i=1}^{N_d} w_i \frac{\partial \psi_j{}^{\boldsymbol{d}_i}}{\partial \theta} = \sum_{i=1}^{N_d} w_i \frac{\partial \mathcal{D}^j CNN_m(\mathbf{W_j}, \lambda_j{}^{\vec{d}_i}, \lambda_{j\,max}{}^{\vec{d}_i})}{\partial \theta} \leq 0,$$
$$for\ j = 1, 2, \dots, N_s, \tag{B.9}$$

If weights that connect the input of $\lambda_{j_{max}}$ to other neurons are negative, the thermodynamic consistency condition is maintained by the proposed model.

Appendix C. Integration point of micro-sphere approach

See Table C.1.

References

[1] Dargazany R, Itskov M. A network evolution model for the anisotropic mullins effect in carbon black filled rubbers. Int J Solids Struct 2009;46(16):2967–77.

[2] Bahrololoumi A, Ghaderi A, Shaafaey M, Dargazany R. A micro-mechanical constitutive model to predict hygrothermal aging of cross-linked polymers. In: ASME international mechanical engineering congress and exposition. Vol. 85680. American Society of Mechanical Engineers; 2021, V012T12A039.

[3] Celina M, Gillen KT, Assink R. Accelerated aging and lifetime prediction: Review of non-arrhenius behaviour due to two competing processes. Polym Degrad Stab 2005;90(3):395–404.

[4] Abdelaziz MN, Ayoub G, Colin X, Benhassine M, Mouwakeh M. New developments in fracture of rubbers: Predictive tools and influence of thermal aging. Int J Solids Struct 2019;165:127–36.

[5] Mengistu T, Pazur RJ. The thermal oxidation of hydrogenated acrylonitrile-co-butadiene rubber from ambient to 150° C. Polym Degrad Stab 2021;188:109574.

[6] Pazur RJ, Petrov I. The thermo-oxidation of isoprene containing copolymers of isobutylene: Activation energies and reactions from room temperature to 100° C. Polym Degrad Stab 2015;113:55–65.

[7] Mohammadi H, Dargazany R. A micro-mechanical approach to model thermal induced aging in elastomers. Int J Plast 2019;118:1–16.

[8] Mohammadi H, Morovati V, Poshtan E, Dargazany R. Understanding decay functions and their contribution in modeling of thermal-induced aging of cross-linked polymers. Polym Degrad Stab 2020;109108.

[9] Bahrololoumi A, Morovati V, Poshtan EA, Dargazany R. A multi-physics constitutive model to predict quasi-static behaviour: Hydrolytic aging in thin cross-linked polymers. Int J Plast 2020;102676.

[10] Shaafaey M, Bahrololoumi A, Mohammadi H, Alazhary S, Dargazany R. Investigation of hygrothermal aging on the polyurethane-based (PUB) adhesive: substantiating competition scenario between sub-aging thermo-oxidation and hydrolytic phenomena. J Polym Res 2021;28(12):1–25.

[11] Bahrololoumi A, Morovati V, Shaafaey M, Dargazany R. A multi-physics approach on modeling of hygrothermal aging and its effects on constitutive behavior of cross-linked polymers. J Mech Phys Solids 2021;156:104614.

[12] Lion A, Johlitz M. On the representation of chemical ageing of rubber in continuum mechanics. Int J Solids Struct 2012;49(10):1227–40.

[13] Gillen KT, Bernstein R, Celina M. Non-arrhenius behavior for oxidative degradation of chlorosulfonated polyethylene materials. Polym Degrad Stab 2005;87(2):335–46.

[14] Celina MC. Review of polymer oxidation and its relationship with materials performance and lifetime prediction. Polym Degrad Stab 2013;98(12):2419–29.

[15] Steinke L, Veltin U, Flamm M, Lion A, Celina M. Numerical analysis of the heterogeneous ageing of rubber products. In: Constitutive models for rubber. Vol. 7. 2011, p. 155–60.

[16] Celina M, Wise J, Ottesen D, Gillen K, Clough R. Oxidation profiles of thermally aged nitrile rubber. Polym Degrad Stab 1998;60(2–3):493–504.

[17] Shaw JA, Jones AS, Wineman AS. Chemorheological response of elastomers at elevated temperatures: experiments and simulations. J Mech Phys Solids 2005;53(12):2758–93.

[18] Huneau B, Le Cam J-B, Marco Y, Verron E. Constitutive models for rubber XI: proceedings of the 11th European conference on constitutive models for rubber (ECCMR 2019), June 25-27, 2019, Nantes, France. CRC Press; 2019.

[19] Zhang M, Sun B, Gu B. Meso-structure ageing mechanism of 3-D braided composite's compressive behaviors under accelerated thermo-oxidative ageing environment. Mech Mater 2017;115:47–63.

[20] Zhang M, Sun B, Gu B. Experimental and numerical analyses of matrix shrinkage and compressive behavior of 3-D braided composite under thermo-oxidative ageing conditions. Compos Struct 2018;204:320–32.

[21] Duchoslav J, Unterweger C, Steinberger R, Fürst C, Stifter D. Investigation on the thermo-oxidative stability of carbon fiber sizings for application in thermoplastic composites. Polym Degrad Stab 2016;125:33–42.

[22] Slater C, Davis C, Strangwood M. Compression set of thermoplastic polyurethane under different thermal–mechanical-moisture conditions. Polym Degrad Stab 2011;96(12):2139–44.

[23] Farrar D, Gillson R. Hydrolytic degradation of polyglyconate b: the relationship between degradation time, strength and molecular weight. Biomaterials 2002;23(18):3905–12.

[24] Vieira A, Vieira J, Ferra J, Magalhães F, Guedes R, Marques A. Mechanical study of PLA–PCL fibers during in vitro degradation. J Mech Behav Biomed Mater 2011;4(3):451–60.

[25] El Yagoubi J, Lubineau G, Traidia A, Verdu J. Monitoring and simulations of hydrolysis in epoxy matrix composites during hygrothermal aging. Composites A 2015;68:184–92.

[26] Pieniak D, Przystupa K, Walczak A, Niewczas AM, Krzyzak A, Bartnik G, et al. Hydro-thermal fatigue of polymer matrix composite biomaterials. Materials 2019;12(22):3650.

[27] Shockley MF, Muliana AH. Modeling temporal and spatial changes during hydrolytic degradation and erosion in biodegradable polymers. Polym Degrad Stab 2020;180:109298.

[28] Loh XJ, Goh SH, Li J. Hydrolytic degradation and protein release studies of thermogelling polyurethane copolymers consisting of poly [(R)-3-hydroxybutyrate], poly (ethylene glycol), and poly (propylene glycol). Biomaterials 2007;28(28):4113–23.

[29] Johlitz M, Diercks N, Lion A. Thermo-oxidative ageing of elastomers: A modelling approach based on a finite strain theory. Int J Plast 2014;63:138–51.

[30] Ogden RW. Large deformation isotropic elasticity–on the correlation of theory and experiment for incompressible rubberlike solids. Proc R Soc Lond Ser A Math Phys Eng Sci 1972;326(1567):565–84.

[31] Kim B, Lee SB, Lee J, Cho S, Park H, Yeom S, et al. A comparison among Neo-Hookean model, Mooney-Rivlin model, and Ogden model for chloroprene rubber. Int J Precis Eng Manuf 2012;13(5):759–64.

[32] Šulc P, Pešek L, Bula V, Košina J, Cibulka J. Torsion dissipated energy of hard rubbers as function of hyperelastic deformation energy of the Yeoh model. Appl Comput Mech 2018;12(1).

[33] Elastomerov T, Rezultatov RU, Prilagajanje EPZ. Elastomer testing: The risk of using only uniaxial data for fitting the Mooney-Rivlin hyperelastic-material model. Mater Tehnol 2018;52(1):3–8.

[34] Yang L, Yang L. Note on gent's hyperelastic model. Rubber Chem Technol 2018;91(1):296–301.

[35] Carroll M. A strain energy function for vulcanized rubbers. J Elasticity 2011;103(2):173–87.

[36] Swanson S, Christensen L, Ensign M. Large deformation finite element calculations for slightly compressible hyperelastic materials. Comput Struct 1985;21(1–2):81–8.

[37] Wang MC, Guth E. Statistical theory of networks of non-Gaussian flexible chains. J Chem Phys 1952;20(7):1144–57.

[38] Nateghi A, Dal H, Keip M-A, Miehe C. An affine microsphere approach to modeling strain-induced crystallization in rubbery polymers. Contin Mech Thermodyn 2018;30(3):485–507.

[39] Khiêm VN, Itskov M. Analytical network-averaging of the tube model:: Rubber elasticity. J Mech Phys Solids 2016;95:254–69.

[40] Miehe C, Göktepe S, Lulei F. A micro-macro approach to rubber-like materials—part I: the non-affine micro-sphere model of rubber elasticity. J Mech Phys Solids 2004;52(11):2617–60.

[41] Marckmann G, Verron E, Gornet L, Chagnon G, Charrier P, Fort P. A theory of network alteration for the mullins effect. J Mech Phys Solids 2002;50(9):2011–28.

[42] Dargazany R, Khiêm VN, Navrath U, Itskov M. Network evolution model of anisotropic stress softening in filled rubber-like materials: Parameter identification and finite element implementation. J Mech Mater Struct 2013;7(8):861–85.

[43] Akbari R, Morovati V, Dargazany R. Reverse physically motivated frameworks for investigation of strain energy function in rubber-like elasticity. Int J Mech Sci 2022;107110.

[44] Amores VJ, Benítez JM, Montáns FJ. Data-driven, structure-based hyperelastic manifolds: A macro-micro-macro approach to reverse-engineer the chain behavior and perform efficient simulations of polymers. Comput Struct 2020;231:106209.

[45] Amores VJ, Benítez JM, Montáns FJ. Data-driven, structure-based hyperelastic manifolds: A macro-micro-macro approach. 2019, arXiv preprint arXiv:1903.11545.

[46] Amores VJ, Nguyen K, Montáns FJ. On the network orientational affinity assumption in polymers and the micro–macro connection through the chain stretch. J Mech Phys Solids 2021;148:104279.

[47] Dal H. A comparative study on the hyperelastic constitutive models for rubber. 2018.

[48] Dal H, Açıkgöz K, Badienia Y. On the performance of isotropic hyperelastic constitutive models for rubber-like materials: A state of the art review. Appl Mech Rev 2021;73(2):020802.

[49] Shen Y, Chandrashekhara K, Breig W, Oliver L. Neural network based constitutive model for rubber material. Rubber Chem Technol 2004;77(2):257–77.

[50] Liang G, Chandrashekhara K. Neural network based constitutive model for elastomeric foams. Eng Struct 2008;30(7):2002–11.

[51] Raissi M, Perdikaris P, Karniadakis GE. Physics-informed neural networks: A deep learning framework for solving forward and inverse problems involving nonlinear partial differential equations. J Comput Phys 2019;378:686–707.

[52] Raissi M, Karniadakis GE. Hidden physics models: Machine learning of nonlinear partial differential equations. J Comput Phys 2018;357:125–41.

[53] Kirchdoerfer T, Ortiz M. Data-driven computational mechanics. Comput Methods Appl Mech Engrg 2016;304:81–101.

[54] Nguyen LTK, Keip M-A. A data-driven approach to nonlinear elasticity. Comput Struct 2018;194:97–115.

[55] Amores VJ, Benítez JM, Montáns FJ. Average-chain behavior of isotropic incompressible polymers obtained from macroscopic experimental data. a simple structure-based WYPiWYG model in julia language. Adv Eng Softw 2019;130:41–57.

[56] Ibanez R, Abisset-Chavanne E, Aguado JV, Gonzalez D, Cueto E, Chinesta F. A manifold learning approach to data-driven computational elasticity and inelasticity. Arch Comput Methods Eng 2018;25(1):47–57.

[57] Reimann D, Nidadavolu K, Vajragupta N, Glasmachers T, Junker P, Hartmaier A, et al. Modeling macroscopic material behavior with machine learning algorithms trained by micromechanical simulations. Front Mater 2019;6:181.

[58] Zopf C, Kaliske M. Numerical characterisation of uncured elastomers by a neural network based approach. Comput Struct 2017;182:504–25.

[59] Ghaderi A, Morovati V, Dargazany R. A physics-informed assembly of feed-forward neural network engines to predict inelasticity in cross-linked polymers. Polymers 2020;12(11):2628.

[60] Ghaderi A, Morovati V, Dargazany R. A Bayesian surrogate constitutive model to estimate failure probability of elastomers. Mech Mater 2021;162:104044.

[61] Ghaderi A, Morovati V, Bahrololoumi A, Dargazany R. A physics-informed neural network constitutive model for cross-linked polymers. In: ASME international mechanical engineering congress and exposition. Vol. 84607. American Society of Mechanical Engineers; 2020, V012T12A007.

[62] Choi HJ, Kim CA, Sohn J-I, Jhon MS. An exponential decay function for polymer degradation in turbulent drag reduction. Polym Degrad Stab 2000;69(3):341–6.

[63] Hutson R, Dowding C. Joint asperity degradation during cyclic shear. Int J Rock Mech Min Sci Geomech Abstr 1990;27(2):109–19.

[64] Bizeul M, Bouvet C, Barrau J-J, Cuenca R. Influence of woven ply degradation on fatigue crack growth in thin notched composites under tensile loading. Int J Fatigue 2010;32(1):60–5.

[65] Ha-Anh T, Vu-Khanh T. Prediction of mechanical properties of polychloroprene during thermo-oxidative aging. Polym Test 2005;24(6):775–80.

[66] Johlitz M. On the representation of ageing phenomena. J Adhes 2012;88(7):620–48.

[67] Mohammadi H, Morovati V, Korayem A-E, Poshtan E, Dargazany R. Constitutive modeling of elastomers during photo-and thermo-oxidative aging. Polym Degrad Stab 2021;191:109663.

[68] Dippel B, Johlitz M, Lion A. Ageing of polymer bonds: a coupled chemomechanical modelling approach. Contin Mech Thermodyn 2014;26(3):247–57.

[69] Vieira AC, Guedes RM, Tita V. Damage-induced hydrolyses modelling of biodegradable polymers for tendons and ligaments repair. J Biomech 2015;48(12):3478–85.

[70] Vieira AC, Guedes RM, Tita V. Constitutive modeling of biodegradable polymers: Hydrolytic degradation and time-dependent behavior. Int J Solids Struct 2014;51(5):1164–74.

[71] Breche Q, Chagnon G, Machado G, Nottelet B, Garric X, Girard E, et al. A non-linear viscoelastic model to describe the mechanical behavior's evolution of biodegradable polymers during hydrolytic degradation. Polym Degrad Stab 2016;131:145–56.

[72] Diani J, Fayolle B, Gilormini P. A review on the mullins effect. Eur Polym J 2009;45(3):601–12.

[73] Zhong D, Xiang Y, Yin T, Yu H, Qu S, Yang W. A physically-based damage model for soft elastomeric materials with anisotropic mullins effect. Int J Solids Struct 2019;176:121–34.

[74] Wan H, Gao K, Li S, Zhang L, Wu X, Wang X, et al. Chemical bond scission and physical slippage in the mullins effect and fatigue behavior of elastomers. Macromolecules 2019;52(11):4209–21.

[75] Bueche F. Molecular basis for the mullins effect. J Appl Polym Sci 1960;4(10):107–14.

[76] Hanson DE, Hawley M, Houlton R, Chitanvis K, Rae P, Orler EB, et al. Stress softening experiments in silica-filled polydimethylsiloxane provide insight into a mechanism for the mullins effect. Polymer 2005;46(24):10989–95.

[77] Musil B, Johlitz M, Lion A. On the ageing behaviour of NBR: chemomechanical experiments, modelling and simulation of tension set. Contin Mech Thermodyn 2018;1–17.

[78] Gagliardi M, Lenarda P, Paggi M. A reaction-diffusion formulation to simulate EVA polymer degradation in environmental and accelerated ageing conditions. Sol Energy Mater Sol Cells 2017;164:93–106.

[79] Musto P, Ragosta G, Abbate M, Scarinzi G. Photo-oxidation of high performance epoxy networks: correlation between the molecular mechanisms of degradation and the viscoelastic and mechanical response. Macromolecules 2008;41(15):5729–43.

[80] Kodera Y, McCoy BJ. Distribution kinetics of radical mechanisms: reversible polymer decomposition. AIChE J 1997;43(12):3205–14.

[81] Ehrenstein GW, Pongratz S. Beständigkeit von kunststoffen. Hanser München; 2007.

[82] Verdu J. Oxydative ageing of polymers. John Wiley & Sons; 2012.

[83] Truesdell C. The elements of continuum mechanics: lectures given in August-September 1965 for the Department of Mechanical and Aerospace Engineering Syracuse University Syracuse, New York. Springer Science & Business Media; 2012.

[84] Ehret A, Itskov M, Schmid H. Numerical integration on the sphere and its effect on the material symmetry of constitutive equations—a comparative study. Internat J Numer Methods Engrg 2010;81(2):189–206.

[85] Bažant P, Oh B. Efficient numerical integration on the surface of a sphere. ZAMM-J Appl Math Mech Z Angew Math Mech 1986;66(1):37–49.

[86] Dal H, Zopf C, Kaliske M. Micro-sphere based viscoplastic constitutive model for uncured green rubber. Int J Solids Struct 2018;132:201–17.

[87] Wang E, Kosson A, Mu T. Deep action conditional neural network for frame prediction in atari games. Technical report, Stanford University; 2017.

[88] Ioannou Y, Robertson D, Zikic D, Kontschieder P, Shotton J, Brown M, et al. Decision forests, convolutional networks and the models in-between. 2016, arXiv preprint arXiv:1603.01250.

[89] Panigrahi A, Shetty A, Goyal N. Effect of activation functions on the training of overparametrized neural nets. 2019, arXiv preprint arXiv:1908.05660.

[90] Hornik K, Stinchcombe M, White H. Multilayer feedforward networks are universal approximators. Neural Netw 1989;2(5):359–66.

[91] Mai T-T, Morishita Y, Urayama K. Novel features of the mullins effect in filled elastomers revealed by stretching measurements in various geometries. Soft Matter 2017;13(10):1966–77.

[92] Dal H, Gültekin O, Açıkgöz K. An extended eight-chain model for hyperelastic and finite viscoelastic response of rubberlike materials: Theory, experiments and numerical aspects. J Mech Phys Solids 2020;145:104159.

[93] Lambert-Diani J, Rey C. New phenomenological behavior laws for rubbers and thermoplastic elastomers. Eur J Mech A Solids 1999;18(6):1027–43.

[94] Le Gac P-Y, Davies P, Choqueuse D. Evaluation of long term behaviour of polymers for offshore oil and gas applications. Oil Gas Sci Technol Rev D'IFP Energies Nouvelles 2015;70(2):279–89.

[95] Stevenson A. On the durability of rubber/metal bonds in seawater. Int J Adhes Adhes 1985;5(2):81–91.